

ISOBARIC VAPOR LIQUID EQUILIBRIUM (VLE)

ACETONE - METHANOL - ETHANOL MIXTURE

CHEG 345 - Chemical Engineering Laboratory I

Lab Instructor: Dr. Douglas J. Buttrey

Group 6 (Just Diene)

Group Leader: Daniel Robinson

Communication Coordinator: Abdul Fayeed Abdul Kadir

Data Coordinator: Neel Shah

Safety and Logistics Coordinator: Evan Sciacchitano

March 29th, 2021

College of Engineering, Department of Chemical and Biomolecular Engineering
University of Delaware
Newark, Delaware 19711

ABSTRACT

Analyses on isobaric vapor-liquid equilibrium (VLE) at a pressure of 1.0271 bar for the ternary mixture of acetone-methanol-ethanol are conducted by examining the corresponding binary mixtures of acetone-ethanol, acetone-methanol, and methanol-ethanol VLE behavior individually. The acetone-methanol mixture notably has an azeotrope at $x_{Ace} = 0.763$, the acetone-ethanol mixture does not have an azeotrope but has a K factor approaching near 1 at $x_{Ace} = 0.9$, and the methanol-ethanol mixture does not have any azeotropic tendencies. The experimental data was plotted alongside literature data to identify that the van Laar correlative model best represents the binary systems and consequently, the ternary system as well. Using the van Laar model to plot liquid phase mole fraction for the ternary system under various isotherms, it was identified that there was no azeotropic composition for the ternary system. The study concludes that distillation of the ternary system due to the differences in relative volatilities of the three components is entirely possible.

TABLE OF CONTENTS

Abstract	1
List of Figures	3
List of Tables	5
Nomenclature	6
Introduction	7
Procedure	8
Results and Discussion	10
Conclusions and Recommendations	25
References	27
Appendices	
Appendix A - <i>Activity Coefficient Predicted by UNIFAC and van Laar Model for Each Binary</i>	28
Appendix B - <i>Quadratic Fitting of van Laar Model with Sinusoidal Error in Fitting</i>	29
Appendix C - <i>Poynting Pressure and Fugacity Coefficient Corrections</i>	32
Appendix D - <i>Injection Data for All Binary Mixtures with their Associated Errors</i>	34
Appendix E - <i>Variations between Atmospheric and Lab Pressure</i>	36
Appendix F - <i>Relevant Antoine Parameters and Compound Thermodynamic Properties</i>	38
Appendix G - <i>Averaged Temperature Data for Each Binary Mixture</i>	39
Appendix H - <i>Experimental Data Fitted to Quadratic Equation, with van Laar and Wilson Correlative Models of T-xy plots</i>	41
Appendix I - <i>T-xy Plots Generated Pre-lab from UNIFAC Predictive Models</i>	43
Appendix J - γ_i^∞ and <i>van Laar Parameters from UNIFAC Predictive Models</i>	44
Appendix K - <i>Contour Plots of the Ternary Mixture on a Ternary Plot For Each Compound</i>	45
Appendix L - <i>Isosurface of the Ternary Mixture on a Ternary Plot</i>	47
Appendix M - <i>MATLAB Coding for Analysis and Plot Generations</i>	47

LIST OF FIGURES

Main Body

Figure 1: Temperature variations in AM mixture as a function of time; a) acetone injected into methanol (left) and b) methanol injected into acetone (right).

Figure 2: Temperature variations in ME mixture as a function of time; a) methanol injected into ethanol (left) and b) ethanol injected into methanol (right).

Figure 3: Temperature variations in AE mixture as a function of time; a) acetone injected into ethanol (left) and b) ethanol injected into acetone (right).

Figure 4: T-xy plot for AM mixture comparing literature data ($\square - x_A^2$, $\blacksquare - y_A^2$ at $P = 1.013$ bar and $\diamond - x_A^3$, $\blacklozenge - y_A^3$ at $P = 1.013$ bar) and experimental data ($\triangle - x_A$, $\blacktriangle - y_A$ at $P = 1.0271$ bar) based on the van Laar and Wilson models ($-x_A$, $--y_A$).

Figure 5: T-xy plot for ME mixture comparing literature data ($\square - x_A^4$, $\blacksquare - y_A^4$ at $P = 0.9987$ bar and $\diamond - x_A^3$, $\blacklozenge - y_A^3$ at $P = 1.013$ bar) and experimental data ($\triangle - x_A$, $\blacktriangle - y_A$ at $P = 1.0271$ bar) based on the van Laar and Wilson models ($-x_A$, $--y_A$).

Figure 6: T-xy plot for AE mixture comparing literature data ($\square - x_A^3$, $\blacksquare - y_A^3$ at $P = 1.013$ bar and $\diamond - x_A^5$, $\blacklozenge - y_A^5$ at $P = 1.013$ bar) and experimental data ($\triangle - x_A$, $\blacktriangle - y_A$ at $P = 1.0271$ bar) based on the van Laar and Wilson models ($-x_A$, $--y_A$).

Figure 7: y-x plot for AM mixture comparing literature data (\blacksquare^2 at $P = 1.013$ bar, \diamond^3 at $P = 1.013$ bar) and experimental data (\circ at $P = 1.0271$ bar) to the van Laar model.

Figure 8: y-x plot for ME mixture comparing literature data (\blacksquare^4 at $P = 0.9987$ bar, \diamond^2 at $P = 1.013$ bar) and experimental data (\circ at $P = 1.0271$ bar) to the van Laar model.

Figure 9: y-x plot of AE mixture comparing literature data (\blacksquare^3 at $P = 1.013$ bar, \diamond^5 at $P = 1.013$ bar) and experimental data (\circ at $P = 1.0271$ bar) to the van Laar model.

Figure 10: Ternary diagram of contour plots of $K = 1$ ($-K_{Ace} = 1$, $--K_{Met} = 1$) of the ternary mixture at $P = 1.0271$ bar.

Figure 11: Ternary diagram of contour plots of various temperatures of the ternary mixture at $P = 1.0271$ bar.

Appendix

Figure A1: Activity Coefficient of Each Binary Pair by UNIFAC Method. AM, ME, and AE respectively.

Figure A2: Activity Coefficient of Each Binary Pair by van Laar Method. AM, ME, and AE respectively.

Figure B1: Fitted Quadratic Model to van Laar Equation of AM mixture pre-lab.

Figure B2: Sinusoidal Plot of Error in Fitting for AM mixture pre-lab.

Figure B3: Fitted Second Order Polynomial to van Laar Equation of ME mixture pre-lab.

Figure B4: Sinusoidal Plot of Error in Fitting for ME mixture pre-lab.

Figure B5: Fitted Second Order Polynomial to van Laar Equation of AE Mixture pre-lab.

Figure B6: Sinusoidal Plot of Error in Fitting for A mixture pre-lab.

Figure C1: Poynting Pressure Correction for All Compounds within 320K - 360K.

Figure C2: Fugacity Coefficient Correction at Varying Temperature for Each Compound.

Figure E1: Recorded Lab Pressure and Atmospheric pressure vs Time on February 25th, 2021.

Figure E2: Recorded Lab Pressure and Atmospheric pressure vs Time on March 5th, 2021.

Figure E3: Recorded Lab Pressure and Atmospheric Pressure vs Time on March 8th, 2021.

Figure E4: Recorded Lab Pressure and Atmospheric Pressure vs Time on March 9th, 2021.

Figure G1: Various averaged temperature data at steady state as a function of time for AM mixture; a) acetone injected into methanol and b) methanol injected into acetone.

Figure G2: Various averaged temperature data at steady state as a function of time for ME mixture; a) methanol injected into ethanol and b) ethanol injected into methanol.

Figure G3: Various averaged temperature data at steady state as a function of time for AE mixture; a) acetone injected into ethanol and b) ethanol injected into acetone.

Figure H1: T-xy plot with quadratic fitting (— x_A , --- y_A) of the experimental data (\triangle - x_A , \blacktriangle - y_A at $P = 1.0271$ bar) for AM mixture; a) A injected into M (left) and b) M injected into A (right).

Figure H2: T-xy plot with quadratic fitting (— x_A , --- y_A) of the experimental data (\triangle - x_A , \blacktriangle - y_A at $P = 1.0271$ bar) for ME mixture; a) M injected into E (left) and b) E injected into M (right).

Figure H3: T-xy plot with quadratic fitting (— x_A , --- y_A) of the experimental data (\triangle - x_A , \blacktriangle - y_A at $P = 1.0271$ bar) for AE mixture; a) A injected into E (left) and b) E injected into A (right).

Figure I1: T-xy of AM Mixture by van Laar Method based on UNIFAC models of infinite dilution activity coefficients.

Figure I2: T-xy of ME Mixture by van Laar Method based on UNIFAC models of infinite dilution activity coefficients.

Figure I3: T-xy of AE Mixture by van Laar Method based on UNIFAC models of infinite dilution activity coefficients.

Figure K1: Ternary diagram of contour plots of various K factors of acetone of the ternary mixture at $P = 1.0271$ bar.

Figure K2: Ternary diagram of contour plots of various K factors of methanol of the ternary mixture at $P = 1.0271$ bar.

Figure K3: Ternary diagram of contour plots of various K factors of ethanol of the ternary mixture at $P = 1.0271$ bar.

Figure L: Isosurface on a Ternary Plot of the Ternary Mixture.

LIST OF TABLES

Main Body

Table 1: Temperature and Pressure offsets for Each Binary Mixture.

Table 2: Percentage of Mass Loss Post Experiment for Each Mixture.

Table 3: Quadratic Equation Fitted to Experimental Data.

Table 4: Calculated Activity Coefficients with Errors for Binary Mixtures.

Table 5: Binary Parameters of van Laar and Wilson model with Errors for Binary Mixtures

Appendices

Table D1: Injection Data and Error Propagation of AM mixture.

Table D2: Injection Data and Error Propagation of ME mixture.

Table D3: Injection Data and Error Propagation of AE mixture.

Table F: Antoine Equation Parameters and Other Thermodynamic Properties.⁸

Table J: γ_i^∞ from UNIFAC models and van Laar Parameters for pre-lab analysis.

NOMENCLATURE

A_t, B_t, C_t	Antoine equation parameters
$\underline{G}', \underline{G}''$	Molar Gibbs free energy at phase I and II
K_i	K factor of species i
P	Pressure (Pa or bar)
$P_i^{vap}(T)$	Vapor pressure as a function of temperature for species i (Pa or bar)
R	Universal gas constant ($8.314 \frac{J}{mol \cdot K}$)
T	Temperature (°C or K)
V_i^L	Liquid molar volume of species i
AM	Acetone-Methanol binary mixture
ME	Methanol-Ethanol binary mixture
AE	Acetone-Ethanol binary mixture
VLE	Vapor-Liquid Equilibrium
\tilde{f}_i^I	Fugacity of species i in phase I (Pa or bar)
x_i	Liquid phase mole fraction of species i
y_i	Vapor phase mole fraction of species i
γ_i	Activity coefficient of species i
γ_i^∞	Activity coefficient of species i at infinite dilution
σ_i	Error of measurement for quantity i
A_{ij}	van Laar Model interaction parameters
Λ_{ij}	Wilson Model interaction parameters
Φ_i	Fugacity coefficient of species i
$\Phi_{sat,i}$	Fugacity coefficient of species i at saturation

INTRODUCTION

Distillation is one of the most important processes in the modern-day industry allowing engineers to purify and separate chemicals from one another. Distillation works by the application and removal of heat to exploit differences in relative volatility. An understanding of the composition of the various phases as a function of temperature, pressure, and mole-fractions is needed to have a successful distillation. This information can be obtained directly through the use of a recirculating still with complex measurement tools to determine equilibrium temperature, pressure, and molar composition of the vapor and liquid phases. A less complete but easier method for obtaining the data is to operate the experiment at either isobaric or isothermal conditions. Boiling temperatures are a function of molar composition and the variable condition, either temperature or pressure, and can be measured to obtain $T - x$ or $P - x$ data respectively. The objective of this experiment is to determine the isobaric vapor-liquid equilibrium (VLE) of the acetone-methanol-ethanol ternary system mixture by analyzing the three binary mixtures separately; acetone-methanol (AM), methanol-ethanol (ME), and acetone-ethanol (AE). For the isobaric case, $T - x$ data will be obtained leading to $x - y$ and $T - x - y$ phase diagrams. Swietoslawski ebulliometers will be used to achieve vapor-liquid equilibrium at ambient pressure with the boiling temperature being measured as a function of the liquid phase composition near the limits of infinite dilution.¹ Using regression analysis from the experimental data, calculated activity coefficients will be used in models such as van Laar and Wilson to demonstrate the behavior over the entire composition range and construct binary phase diagrams. From the combined data of all three binary mixtures, a correlative model will be selected as the best representation of the ternary mixture VLE behavior allowing for proper modeling of distillation.

In order to identify VLE in the multiple systems, the criteria for equilibrium needs to be considered and examined. The main criteria for equilibrium is that the two phases have the same molar Gibbs energy, $\underline{G}^I = \underline{G}^{II}$. When examining this criteria for the equilibrium between the vapor and liquid phases, it becomes $\underline{G}^L(T, P) = \underline{G}^V(T, P)$ where molar Gibbs energy is a function of temperature and pressure. This criteria then leads to a subsequent criteria that VLE occurs when the fugacities of the vapor and liquid phases are equal. This relation is shown in Eq. 1, which further expands to Eq. 2.

$$\underline{f}_i^L(T, P, \underline{x}) = \underline{f}_i^V(T, P, \underline{y}) \quad \text{Eq. 1}$$

$$x_i \gamma_i^L(T, P, \underline{x}) P_i^{vap}(T) \Phi_{sat,i} \exp \left\{ \frac{V_i^L [P_{total} - P_i^{vap}(T)]}{RT} \right\} = y_i P_{total} \Phi_i^V \quad \text{Eq. 2}$$

This is the fundamental criteria for equilibrium that will be considered in this report as the liquid phase and vapor phase fugacities can be calculated for the sets of binary mixtures as well as ultimately for the ternary mixture to determine when VLE occurs.

PROCEDURE

This experiment was not conducted by the group in person due to the COVID-19 pandemic and as such the experimental data was provided by the TAs. This experiment was conducted using four ebulliometers allowing for four different sets of binary mixtures to be examined at once. Since this experiment was conducted over multiple days, all six pairs of solute/solvent combinations were examined experimentally. The bottom of the ebulliometer is the boiler which is wrapped in heating tape with a thermal coupler between the tape and the outer wall of the boiler allowing for the heating to be controlled by the Proportional Integral Derivative (PID) controller above.¹ Typically this temperature is set between 40°C - 50°C higher than the anticipated boiling point, allowing for the solvent to boil in an appropriate time limit as well as not disrupting the condenser with violent boiling. The middle of the ebulliometer contains thermal well and control pumps which are surrounded by insulation. The thermal well is filled with oil to keep temperature stable and unaffected by the environment. The Resistance Temperature Detector (RTD) sensor will then be inserted into the top of the thermal well to measure vapor phase temperature.¹ A barometer at the top of the ebulliometer is used to track barometric pressure for error calculations in data analysis. To analyze a binary mixture, the solvent was extracted with a syringe and then injected into the ebulliometer at the injection point. The specific injection size limits of the solute were determined before the experiment by running ASPEN simulations for the binary mixtures to obtain infinite dilution parameters which were used in the van Laar equation. **Figure A1 and A2 in Appendix A** show the plot of activity coefficients predicted by UNIFAC and van Laar method respectively for each binary mixture. From there a quadratic fit was applied to the van Laar model and a molar concentration was selected to maintain a sinusoidal error in the range of ± 0.005 K of the $T_{\text{vanLaar}} - T_{\text{Quadratic}}$ in **Appendix B**, which helps determine the size of solute injected at each time interval. The precise amount of solute injected into the ebulliometer is crucial for the experiment and as such, the syringe was weighed before and after injection to find the mass of solvent/solute used by difference. When the experiment was finished, the liquid in the ebulliometer was collected by opening a stopcock at the bottom of the boiler. This liquid was then weighed to check that approximately 95% or more of the injected liquid was present in order to conclude that the measurements taken at the beginning leads to less errors in data analysis.

Methanol and ethanol used in the experiment were both 99.9% pure. Two different sets of acetone were used, where acetone with 99.7% purity was used for the AM mixture experiment, while 99.5% purity was used for AE setups. Due to the nature of the chemicals used, this experiment has many safety precautions that would need to be considered. All three chemicals are highly flammable in both liquid and vapor phases, meaning that experimenters need to use spark proof appliances, take precautions against electrostatic charges, keep mixtures away from naked flames and heat, and measure solvent/solute concentration in the air regularly. All three chemicals have specific health hazards associated with them and will be discussed individually. Acetone is very irritating to mucous membranes leading to upper respiratory tract discomfort and difficulty in breathing when inhaled or ingested. Acetone is also irritating to skin and eyes when exposed to concentrated amounts or for a prolonged period of time. Meanwhile, ethanol exposure via inhalation and skin contact may cause irritation to the eyes, dryness or cracking of the skin, irritation to the respiratory tract, and headaches. Aside from that, methanol exposure via ingestion or inhalation may cause eye irritation, headaches, fatigue, drowsiness, and can produce

central nervous system depression and optic nerve damage at high levels of exposure. Due to the dangers associated with methanol and acetone, proper personal protective equipment (PPE) should be worn and breaks should be taken if needed. If an experimenter is exposed, call UD police and follow lab safety precautions in accordance with the type of exposure. Due to the dangers associated with all three chemicals they need to be stored in the proper storage closet seen in the laboratory which has proper ventilation and conditions for them. Disposal of all chemicals should be done in the associated receptacle in the lab and should not be disposed of in the sink or sewage system. The major operational hazards in this experiment come from the sharp syringe, hot boiler, and potential ignition source from electrical wiring. If proper PPE is worn, and the ebulliometer is properly set up with no frayed wires and properly wrapped boiler, then the operational hazards should not be a factor.

RESULTS AND DISCUSSION

The significance of Poynting pressure correction, $\exp\left\{\frac{V_i^L[P_{total} - P_i^{vap}(T)]}{RT}\right\}$ and fugacity coefficient corrections, $\frac{\Phi_i^V}{\Phi_{sat,i}}$ in **Eq. 2** were determined as shown in **Appendix C**. It was found that the Poynting pressure is negligible while the fugacity coefficient corrections should be taken into account into the entire analysis. **Eq. 2** then can further simplify into **Eq. 3**, as shown below.

$$x_i \gamma_i^L(T, P, x_i) P_i^{vap}(T) = y_i P_{total} \left(\frac{\Phi_i^V}{\Phi_{sat,i}} \right) \quad \text{Eq. 3}$$

The experimental data for each binary mixture are tabulated in **Table D1 - D3** in **Appendix D**, with the associated errors in measurement. The temperature and pressure in **Appendix D** have been corrected based on the true temperature and pressure at Newark, Delaware. The corrections were done by first comparing the lab and atmospheric pressure readings on the day the experiment was conducted. The pressure variations plot are included in **Appendix E**, **Figure E1 - E4**. The atmospheric pressures were recorded from the local barometric pressure using the UD College of Agriculture site for the Delaware Environmental Observing System (DEOS). The final pressure used to represent the isobaric system that was examined is 1.0271 bar, which is the average of the true atmospheric pressures from DEOS over the days when the experiment was conducted. From **Figure E1 - E4**, the atmospheric pressure and Antoine correlation from **Eq. 4** were used instead of the lab barometer pressure to calculate the true boiling point of a solvent for each binary because of a small influence from the building's ventilation system and barometer being in the basement.

$$\log_{10} P_i^{vap}(T) = A_t - \frac{B_t}{T+C_t} \quad \text{Eq. 4}$$

Antoine parameters and relevant thermodynamic properties of each compound is as tabulated in **Table F** in **Appendix F**. The differences between the solvent true boiling point and the recorded boiling point by RTD are computed. These offsets are then applied to every temperature data of the injection of solutes, which has been done on the tabulated data in **Table D1 - D3**. The temperature and pressure offsets for each mixture are different and are shown in **Table 1** below.

Table 1: Temperature and Pressure offsets for Each Binary Mixture.

Mixture	Solute	Date	T _{offsets} (°C)	σ _{T,offsets} (°C)	P _{offsets} (bar)	σ _{P,offsets} (bar)
AM	A	2/25/21	0.79	0.22	0.0048	0.0671
	M	2/25/21	-0.25	0.02	0.0044	0.0671
ME	M	3/5/21	-0.11	0.05	0.0048	0.0671
	E	3/9/21	-0.51	0.02	0.0046	0.0671
AE	A	3/9/21	0.18	0.11	0.0044	0.0671
	E	3/8/21	0.07	0.22	0.0046	0.0671

The pressure offsets seen in **Table 1** above are essentially constant with there being slight variation at five significant figures. This is what was expected due to the difference in pressure caused by the lab ventilation and depth being the same throughout the experiment and any true variations in pressure came from atmospheric pressure change. Another important note is that the methanol injected into ethanol experimental data on Mar. 5th had significant error associated with the measurements from the RTD sensor. The first injection of solute was made right away even when the initial recorded solvent boiling point data did not reach a constant value just yet. When computing the average of the last 5 temperature data to calculate the solvent boiling point, it would not reflect the correct ‘recorded boiling point’ of ethanol during that day. This error could come from multiple courses such as variation in the amount of oil the sensor is submerged in, oil temperature not reaching a constant steady state throughout, or any number of electrical errors. Instead, the boiling point of ethanol from Mar. 9th, when acetone was injected into ethanol, was used as the ‘recorded boiling point’ of solvent for Mar. 5th data, and then further corrected based upon the UNIFAC prediction model of T-xy data ($T_{\text{offsets}} = -0.11^\circ\text{C}$). With this correction made and the new temperature offset applied for that day, the data shows similar trends when compared to the other experiments, confirming this was an accurate assessment.

The temperature data tabulated in **Table D1 - D3** for every injection were determined by averaging the last 5 temperature data before the next injection of solute into the mixture, the same way to determine the boiling point of solvent used each day as mentioned previously. This averaging is done consistently to all mixtures to minimize the error in our calculations. The raw temperature data for each mixture varies with time, as depicted in **Figures 1 - 3**.

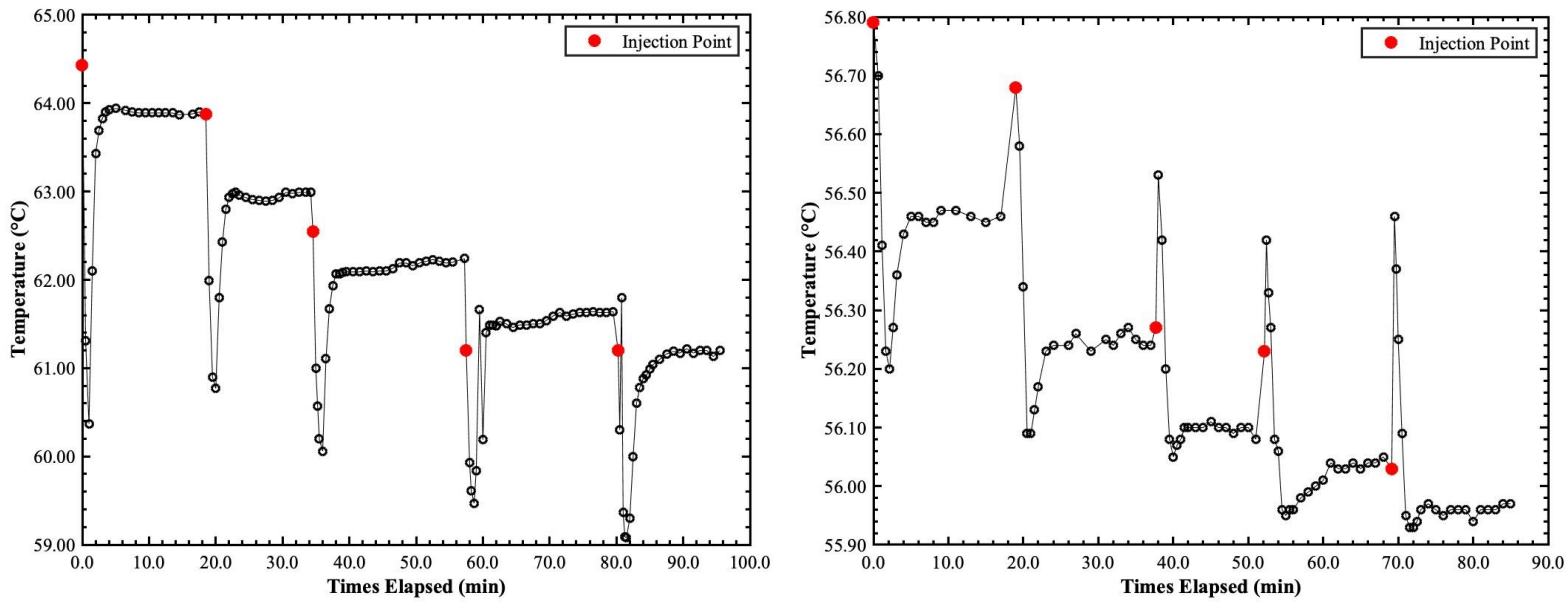


Figure 1: Temperature variations in AM mixture as a function of time; a) acetone injected into methanol (left) and b) methanol injected into acetone (right).

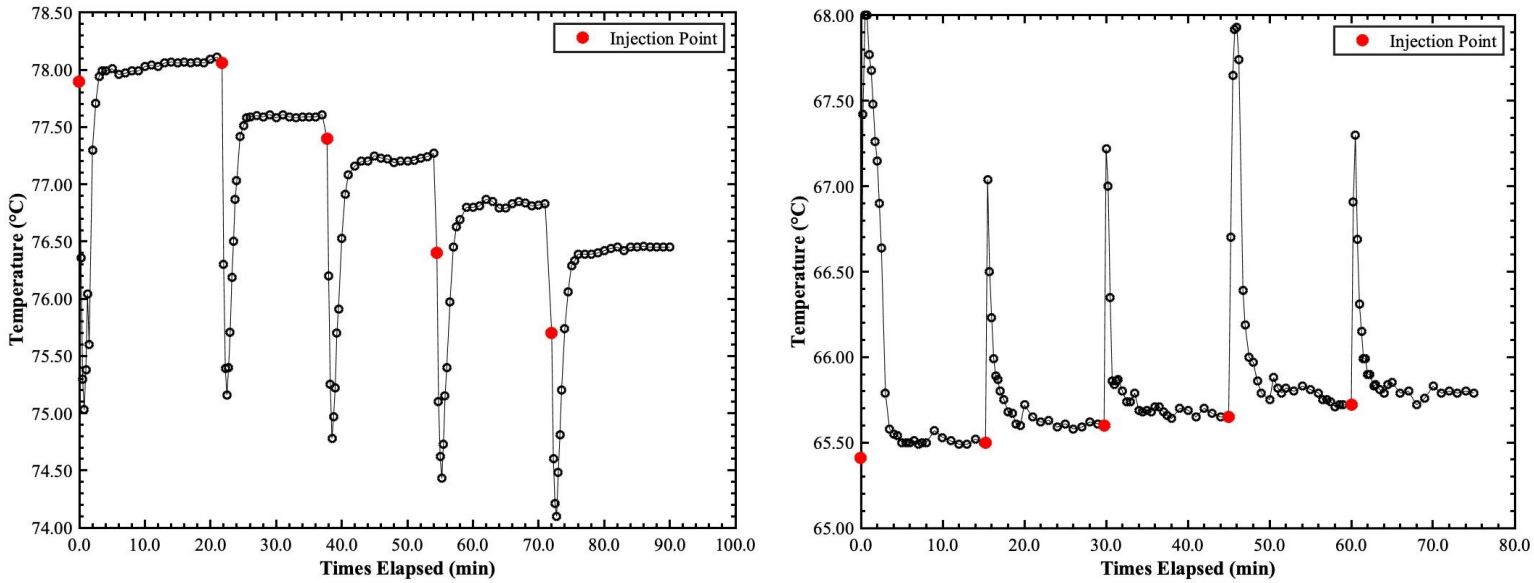


Figure 2: Temperature variations in ME mixture as a function of time; a) methanol injected into ethanol (left) and b) ethanol injected into methanol (right).

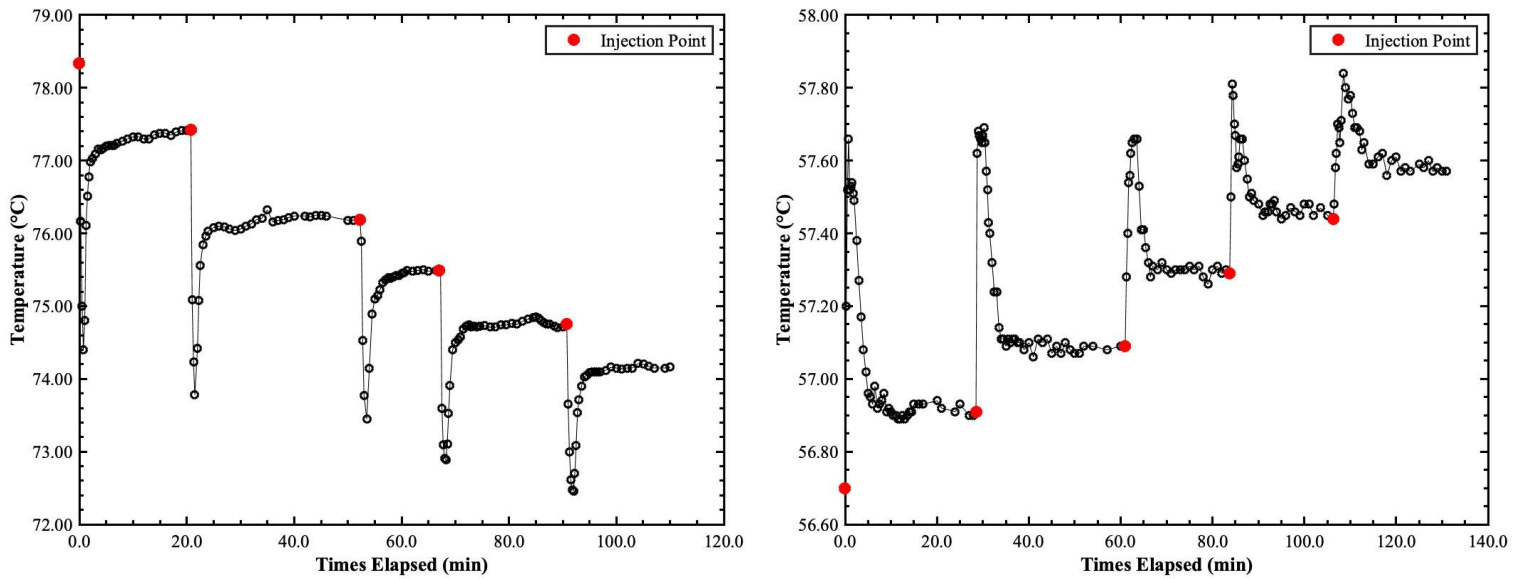


Figure 3: Temperature variations in AE mixture as a function of time; a) acetone injected into ethanol (left) and b) ethanol injected into acetone (right).

In **Figures 1 - 3**, the raw injection temperature data is plotted against time allowing for the injection point to be shown apart from the steady-state temperature values. The injection point values have two distinct trends in these figures. Firstly, the injection point temperature will drop drastically for a brief period of time before rising rapidly to steady-state, and secondly, the temperature will spike rapidly and then decrease rapidly to reach steady state. The first case occurs when a solute with a lower boiling point is injected into a solvent with a higher boiling point. The mixture's overall temperature will then decrease rapidly as this lower temperature solute is mixed with the higher temperature solvent until the mixing is completed and the new mixture's steady-state temperature is reached. **Figure 1a, 2a and 3a** display this trend. In the second case the opposite occurs, a higher boiling point temperature solute is added to solvent with a lower boiling point temperature. This causes the mixture's temperature to jump rapidly as it accommodates this new hotter solute and as mixing finishes, the temperature reaches a steady-state for the new mixture. This trend is as shown in **Figure 1b, 2b and 3b**. Based on these trends, the data for the nonsteady-state mixture data will be excluded moving forward as we care about the steady-state temperature for each mole fraction. The steady-state data was selected by taking the last five temperature points before the next injection as these points will be at a steady-state due to them having the maximum amount of time to achieve this. The temperature offsets are applied to these averaged temperature data, and their variations with time are illustrated in **Figures G1 - G3 in Appendix G**. It is also noted that there is a variation in mass collected post experiments. This variation is tabulated in **Table 2**.

Table 2: Percentage of Mass Loss Post Experiment for Each Mixture.

Mixture	Solute	Actual Mass (g)	Maximum Mass (g)	Mass loss (g)	Percentage Loss (%)
AM	A	44.368	45.993	1.625	3.53
	M	40.758	43.256	2.498	5.77
ME	M	41.573	42.147	0.574	1.36
	E	41.453	41.881	0.428	1.02
AE	A	41.194	41.247	0.053	0.13
	E	41.876	44.073	2.197	4.98

The maximum mass describes the total mass that should be collected after adding the solvent and all 5 injections at the end of the experiment. However, the actual mass collected is less than that and the percentage loss in mass is as shown in **Table 2**. This may be due to some liquid evaporating during injection or collection post experiments. The percentage mass loss is higher when methanol and ethanol are injected into acetone as a solvent when compared to the rest. This is expected because acetone is the most volatile of the three components and therefore there is a large difference in boiling point temperature between the added solute and the steady state temperature of the solution in these scenarios. The temperature and mole fraction tabulated in **Table D1 - D3** are fitted with a quadratic fitting in MATLAB. The quadratic equation for each solute/solvent pair is listed below in **Table 3** in the format of **Eq. 5**.

Table 3: Quadratic Equation Fitted to Experimental Data.

Mixture	Solute	Quadratic Equation
AM	A	$T = 338.95 - 73.77x_A + 296.38x_A^2$
	M	$T = 346.70 - 43.07x_A + 26.00x_A^2$
ME	M	$T = 351.80 - 32.45x_M + 85.27x_M^2$
	E	$T = 322.65 + 39.54x_M - 24.15x_M^2$
AE	A	$T = 352.03 - 115.88x_A + 437.50x_A^2$
	E	$T = 329.97 + 7.80x_A - 7.89x_A^2$

$$T = c + ax_i + bx_i^2; \left(\frac{dT}{dx_i}\right)_{P, x_i \rightarrow 0} = a \quad \text{Eq. 5}$$

The plot of quadratic equations fitted to experimental data, alongside the T-xy plots of van Laar and Wilson model are as attached in **Appendix H**. Further discussion on these plots are provided in **Appendix H**. From these quadratic equations, the activity coefficients at infinite dilution, γ_i^∞ of each species in the binary mixtures can be determined from **Eq. 6**, and the values with their errors are as tabulated in **Table 4**.

$$\gamma_i^\infty = \frac{P_j^{vap}(T) - \left(\frac{dP_i^{vap}(T)}{dT}\right)\left(\frac{dT}{dx_i}\right)_{P, x_i \rightarrow 0}}{P_i^{vap}(T)} \quad \text{Eq. 6}$$

Table 4: Calculated Activity Coefficients with Errors for Binary Mixtures.

<i>ij</i>		γ_i^∞			
1	2	γ_1^∞	$\sigma_{\gamma_1^\infty}$	γ_2^∞	$\sigma_{\gamma_2^\infty}$
Acetone	Methanol	2.2407	0.0012	1.6807	0.0011
Methanol	Ethanol	1.0459	0.0006	1.3578	0.0006
Acetone	Ethanol	1.8334	0.0009	2.0797	0.0014

The value of γ^∞ can be used to solve for the interaction parameters associated with the van Laar model, A_{ij} from **Eq. 7**, and the Wilson model, Λ_{ij} from **Eq. 8**, as tabulated in **Table 5**, with their associated errors.

$$\ln \gamma_i^\infty(x_i \rightarrow 0) = A_{ij} \quad \text{Eq. 7}$$

$$\ln \gamma_i^\infty(x_i \rightarrow 0) = -\ln \Lambda_{ij} + 1 - \Lambda_{ji} \quad \text{Eq. 8}$$

Table 5: Binary Parameters of van Laar and Wilson model with Errors for Binary Mixtures

<i>ij</i>		A_{ij}				Λ_{ij}			
1	2	A_{12}	$\sigma_{A_{12}}$	A_{21}	$\sigma_{A_{21}}$	Λ_{12}	$\sigma_{\Lambda_{12}}$	Λ_{21}	$\sigma_{\Lambda_{21}}$
Acetone	Methanol	0.8068	0.0005	0.5192	0.0006	0.4185	0.0010	1.0642	0.0010
Methanol	Ethanol	0.0449	0.0005	0.3058	0.0004	1.9607	0.0007	0.2818	0.0007
Acetone	Ethanol	0.6062	0.0005	0.7322	0.0007	0.8462	0.0010	0.5608	0.0011

The parameters are then used to solve for the activity coefficient over a range of mole fraction by using **Eq. 9** and **10** for van Laar, and **Eq. 11** and **12** for Wilson model.

$$\ln \gamma_1(x_1) = A_{12} \left[\frac{A_{21}x_2}{A_{12}x_1 + A_{21}x_2} \right]^2 \quad \text{Eq. 9}$$

$$\ln \gamma_2(x_2) = A_{21} \left[\frac{A_{12}x_1}{A_{12}x_1 + A_{21}x_2} \right]^2 \quad \text{Eq. 10}$$

$$\ln \gamma_1 = -\ln(x_1 + x_2 \Lambda_{12}) + x_2 \left[\frac{\Lambda_{12}}{x_1 + x_2 \Lambda_{12}} - \frac{\Lambda_{21}}{x_1 \Lambda_{21} + x_2} \right] \quad \text{Eq. 11}$$

$$\ln \gamma_2 = -\ln(x_2 + x_1 \Lambda_{21}) - x_1 \left[\frac{\Lambda_{12}}{x_1 + x_2 \Lambda_{12}} - \frac{\Lambda_{21}}{x_1 \Lambda_{21} + x_2} \right] \quad \text{Eq. 12}$$

From there, the relationship between the temperature over the same range of mole fraction could be determined through optimization and iteration process in MATLAB from the basis of **Eq. 3**. This is used to produce T-xy plots for each of the binary mixtures individually which were analyzed and discussed below beginning with **Figure 4** which shows the T-xy plot for AM mixture.

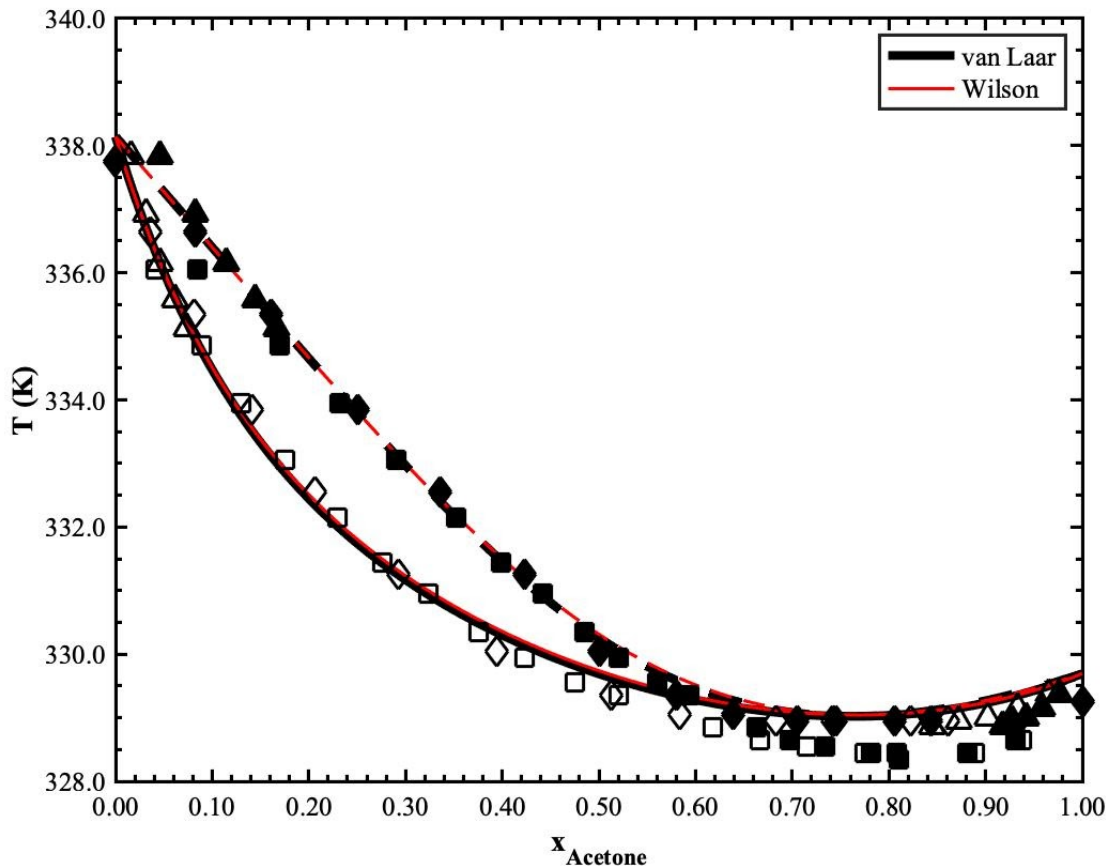


Figure 4: T-xy plot for AM mixture comparing literature data ($\square - x_A^2$, $\blacksquare - y_A^2$ at $P = 1.013$ bar and $\diamond - x_A^3$, $\blacklozenge - y_A^3$ at $P = 1.013$ bar) and experimental data ($\triangle - x_A$, $\blacktriangle - y_A$ at $P = 1.0271$ bar) based on the van Laar and Wilson models ($- - x_A$, $-- y_A$).

Figure 4 compares the data from the van Laar and Wilson model to the experimental data achieved in this lab as well as supporting data from literature sources of a similar experiment. It shows that both models are very accurate in their values for this system and replicate the data trends alongside actual values very well. Data from Tu et al. ($\square \blacksquare$) depicts the same azeotropic behavior, but at a slightly lower temperature, possibly due to lab conditions or procedure of this particular source.² Experimental data and data from Amer et al. ($\diamond \blacklozenge$) match both the models.³ Based on the above figure and comparison, it could be seen that either the van Laar or Wilson model would be able to more accurately predict the values and overall behavior of this binary mixture. This means that moving forward examining the other two binary mixtures, only one of the correlative models is needed to replicate the experimental and literature data trends to model the ternary mixture correctly. As noted above in **Table 1**, the temperature values used in **Figure 4** have been modified according to the systematic temperature error identified and have been shifted to reflect the true temperature rather than the lab readings in order to provide a more accurate data model. As stated above in order to get a more accurate assessment of which model provides the most accurate representation of the ternary model, the T-xy behavior of the ME mixture is analyzed based on **Figure 5** next.

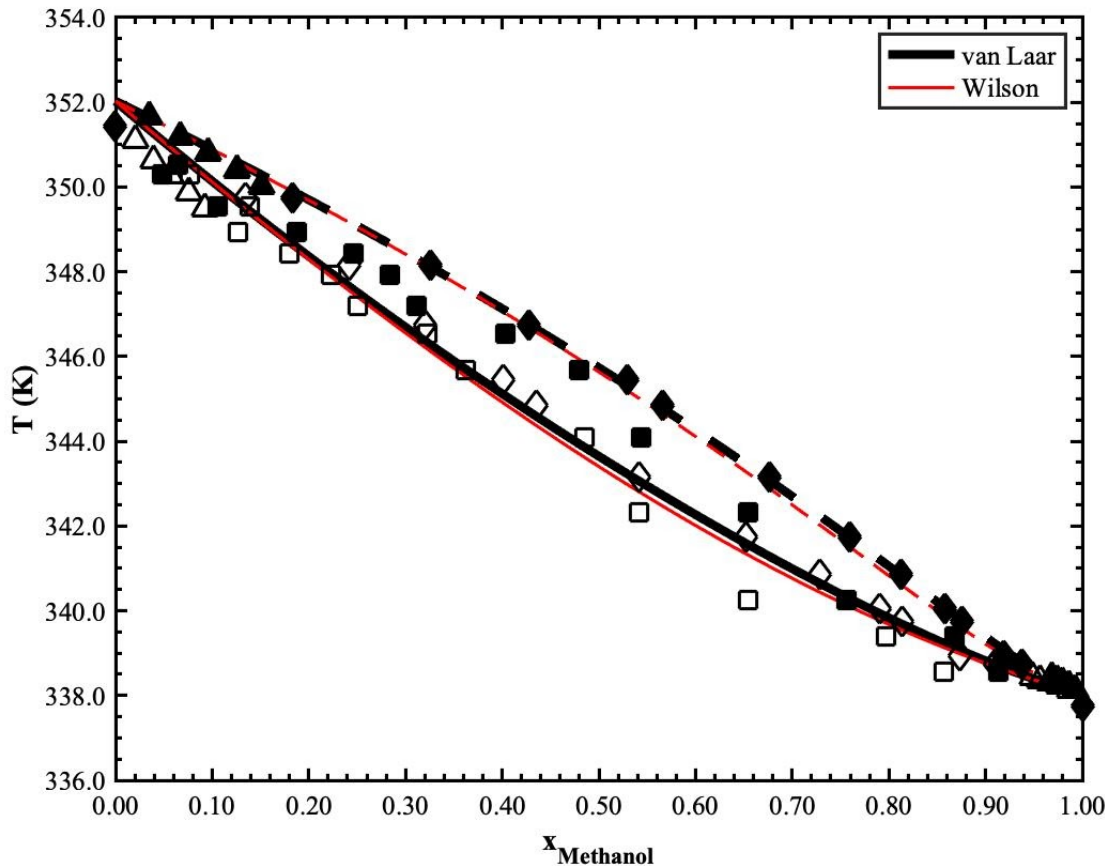


Figure 5: T-xy plot for ME mixture comparing literature data (\square - x_A ⁴, ■ - y_A ⁴ at $P = 0.9987$ bar and \diamond - x_A ³, ♦ - y_A ³ at $P = 1.013$ bar) and experimental data (\triangle - x_A , \blacktriangle - y_A at $P = 1.0271$ bar) based on the van Laar and Wilson models (— x_A , --- y_A).

Figure 5 compares the results from the van Laar and Wilson models for the ME mixture to the experimental data obtained in the lab and to literature data of similar experiments under similar conditions. This yet again shows that both models have very high accuracy in the data for this binary mixture in both the values obtained and the trends of the data. However, in this binary mixture, the van Laar model begins to separate itself from the Wilson model and provides slightly more accurate results due to the Wilson model slightly under predicting the values of both liquid and vapor phases. In the liquid phase, the Wilson model is distinct from the van Laar model and the experimental data in the range of $0.4 \leq x_{\text{Acetone}} \leq 0.7$, and is closer to alignment with a few outliers seen in one of the literature cases, while the van Laar model has a very accurate trend and data results that align with both the experimental data and most of the literature data. From this result it could be seen that the van Laar model is favored as the best fit for the ternary system over the Wilson model. However this cannot be confirmed yet without further examination of the T-xy relationship of the AE mixture seen as depicted in **Figure 6**.

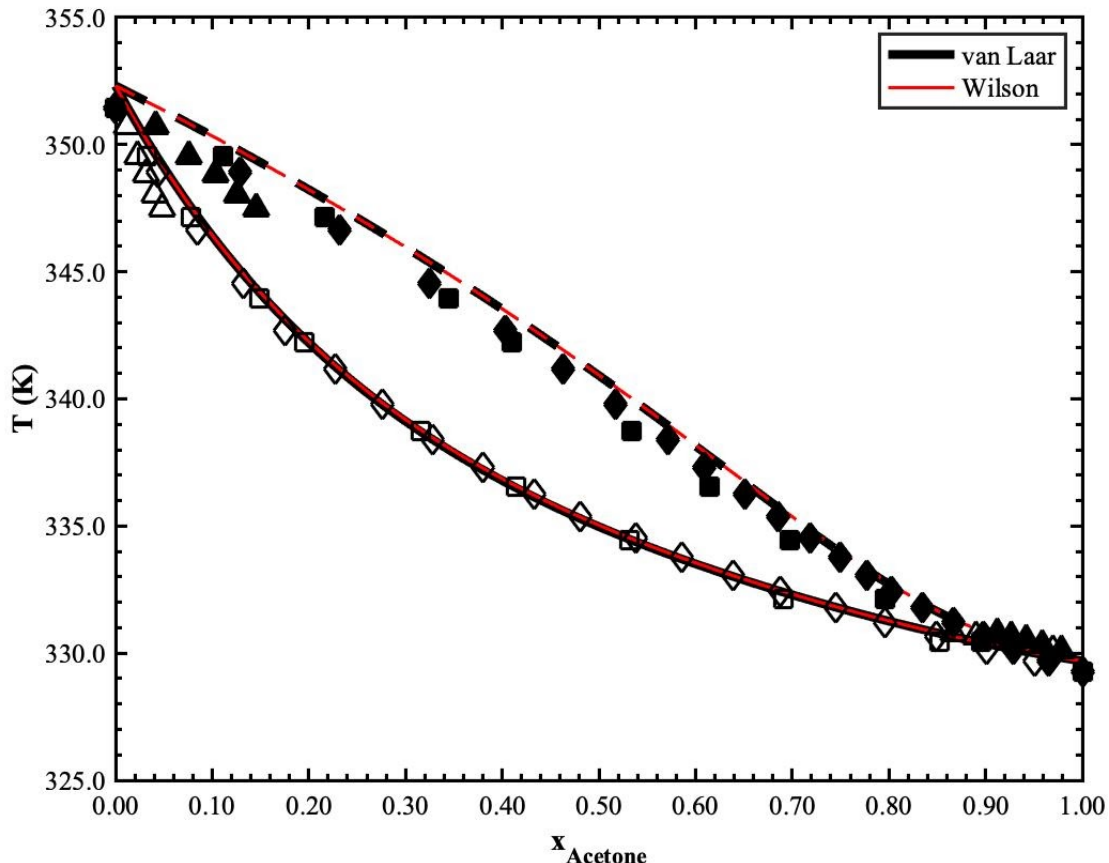


Figure 6: T-xy plot for AE mixture comparing literature data ($\square - x_A^3$, $\blacksquare - y_A^3$ at $P = 1.013$ bar and $\diamond - x_A^5$, $\blacklozenge - y_A^5$ at $P = 1.013$ bar) and experimental data ($\triangle - x_A$, $\blacktriangle - y_A$ at $P = 1.0271$ bar) based on the van Laar and Wilson models ($- x_A$, $-- y_A$).

The predicted behavior by the van Laar and Wilson models in **Figure 6** are both highly accurate for the liquid phase when compared with the literature and experimental data. However, both models do not accurately describe the precise values for the vapor phase data when x_{Acetone} is below 0.60 for either experimental or literature data. Yet, most importantly both the van Laar and Wilson models data trends follow the trends seen in experimental and literature data sets showing that while the precise values may not be perfect away from the infinite-dilution limits, the models are still accurate. This in combination with the conclusions drawn from **Figure 4** and **5** show that the van Laar and Wilson model both are fairly accurate for representing the ternary system but the van Laar model is the most accurate and as such is what will be used for the ternary system phase diagrams analysis. The above T-xy plots from **Figure 4 - 6** can be compared with the T-xy plots initially generated during the pre-lab from the UNIFAC predictive model to find the values of γ_i^∞ in **Appendix I**, with their associated γ_i^∞ and A_{ij} tabulated in **Table J** in **Appendix J**. Further examination of each of the binary mixtures is conducted below with y-x plots allowing for the specific examination of azeotropic tendencies. The AM mixture is examined first from **Figure 7**.

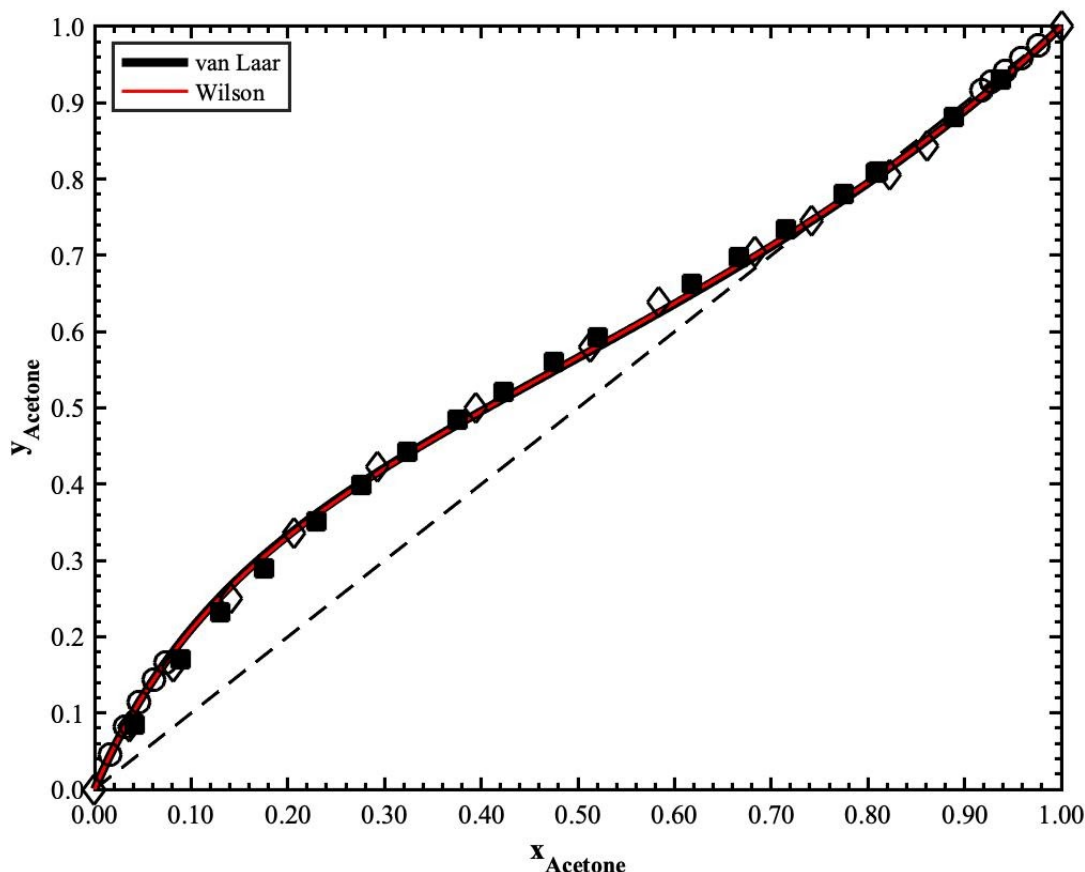


Figure 7: y-x plot for AM mixture comparing literature data (\blacksquare^2 at $P = 1.013$ bar, \diamond^3 at $P = 1.013$ bar) and experimental data (\circ at $P = 1.0271$ bar) to the van Laar model.

Figure 7 elucidates that the AM mixture forms an azeotrope beginning at $x_{\text{Acetone}} = 0.763$, meaning that the vapor and liquid phase molar compositions are equal leading to significant difficulty in separation due to relative volatilities. This difficulty continues up until $x_{\text{Acetone}} = 1$ due to the K factor ($K_i = \frac{y_i}{x_i}$) being extremely close to 1, which indicates an azeotrope and more importantly that the composition is very similar in vapor and liquid phase compositions. In addition, experimental and literature data were plotted alongside both the van Laar and Wilson models showing again that both models have an accurate representation of the y-x behavior of the AM mixture. Following this, the examination of the y-x plot for the ME mixture is conducted to examine its specific molar compositions and any notable azeotropic tendencies as shown in **Figure 8**.

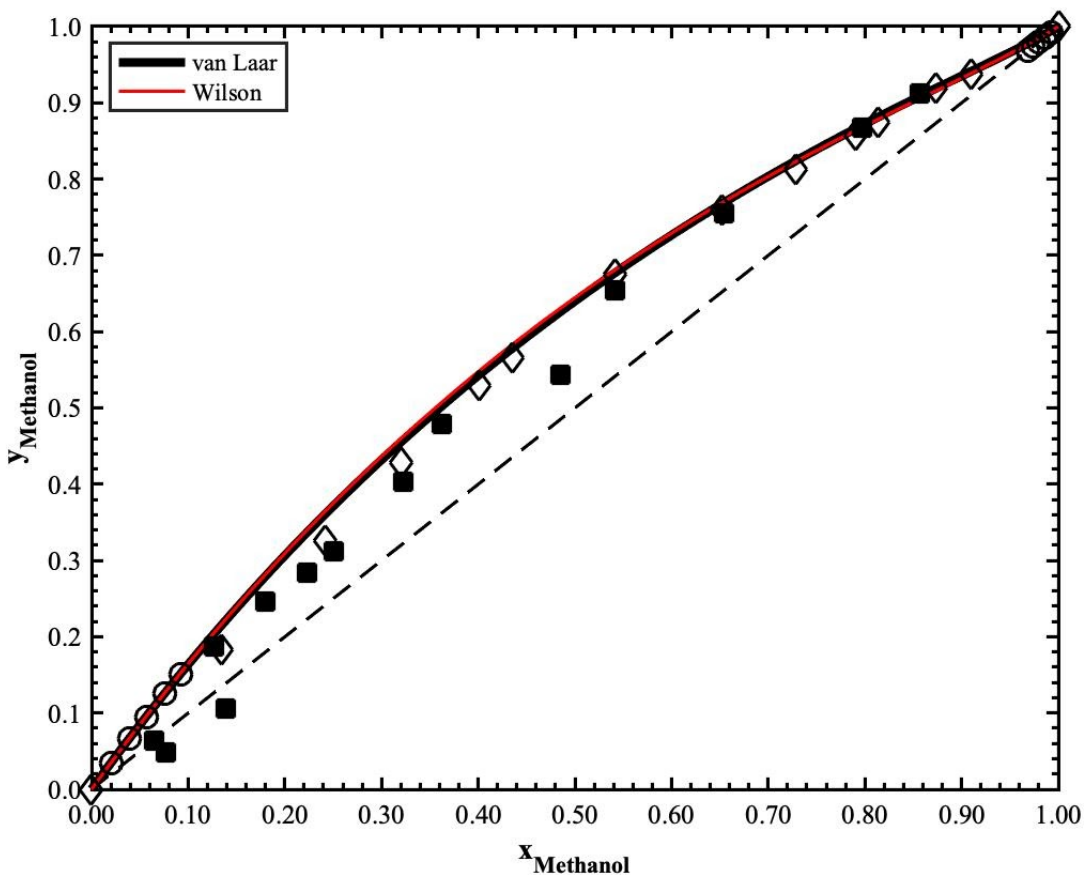


Figure 8: y-x plot for ME mixture comparing literature data (\blacksquare^4 at $P = 0.9987$ bar, \diamond^2 at $P = 1.013$ bar) and experimental data (\circ at $P = 1.0271$ bar) to the van Laar model.

It is shown from **Figure 8** that the mixture does not form an azeotrope under the conditions specified due to the liquid and vapor phase lines having no intersection at the $y = x$ line (--- line in the figure). However this binary mixture has K factors approaching one in the range $0 \leq x_{\text{Methanol}} \leq 0.1$ and $0.8 \leq x_{\text{Methanol}} \leq 1$ indicating that while an azeotrope isn't formed there could potentially be problems in distillation at these mole fractions due to the similarities in volatilities. The literature and experimental data were also plotted alongside the van Laar and Wilson model trend lines. From this it is seen that both literature and experimental data fail to align with each other, but still follow the same trend. Due to the data trends being similar, it could be concluded that the models give an accurate representation of the system and that the lack of an azeotropic composition is an accurate assessment for the ME binary mixture. To finalize examining each of the binary mixtures to obtain a general idea of the ternary mixture behavior, the y-x plot of the AE mixture is analyzed next and as shown in **Figure 9**.

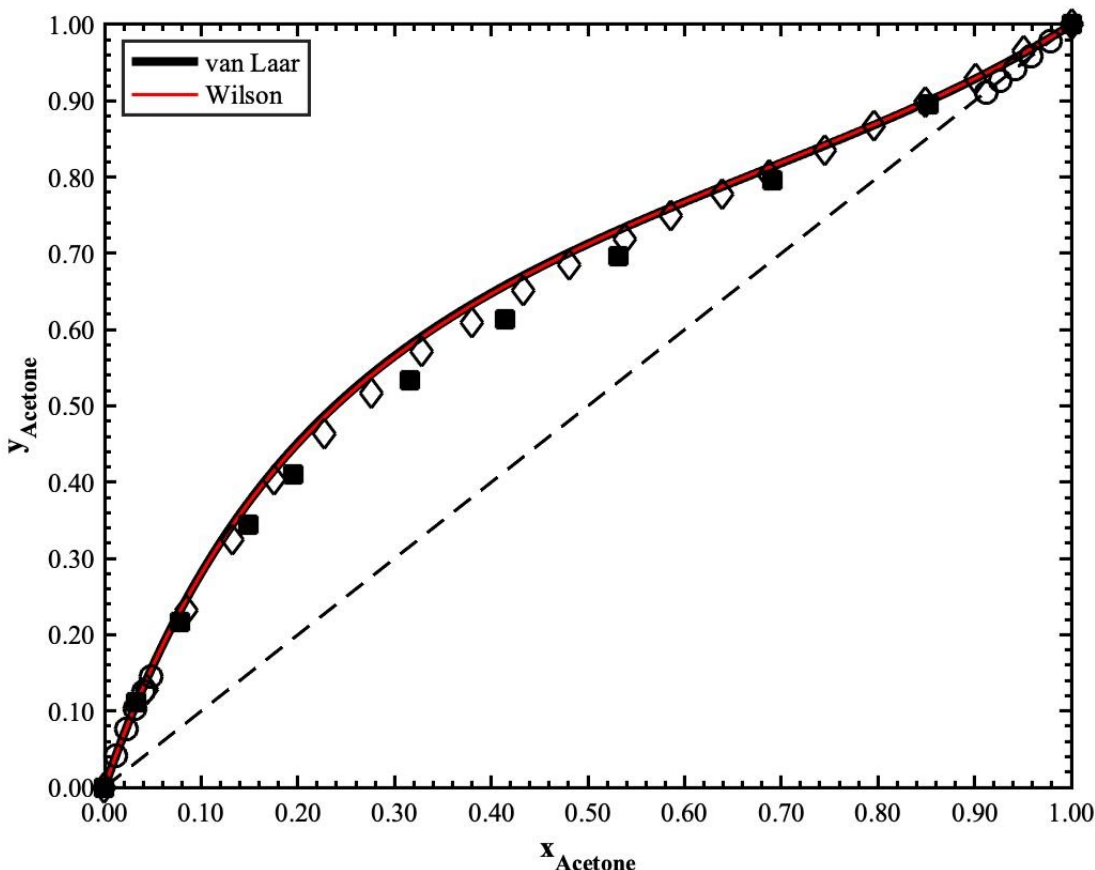


Figure 9: y-x plot of AE mixture comparing literature data (\blacksquare^3 at $P = 1.013$ bar, \diamond^5 at $P = 1.013$ bar) and experimental data (\circ at $P = 1.0271$ bar) to the van Laar model.

The y-x plot for the AE mixture in **Figure 9** generated using the van Laar and Wilson models shows great agreement with both the experimental and literature data. It is compared to confirm that the van Laar model accurately predicts the AE binary mixture. The above figure also shows that the AE binary mixture does not form an azeotrope under the conditions specified. Additionally due to the significant boiling point difference between the two compounds, the K factor is much larger than 1 allowing for easier separation. However, the y-x plot does begin to converge to unity near the acetone-rich end at $x_{\text{Acetone}} = 0.9$, creating a pinching point. With a large fluctuation in temperature and pressure on the experimental setup, this mixture may form an azeotrope, causing great difficulty in separation. With this knowledge, the azeotrope can be prevented from forming by carefully monitoring the temperature and pressure fluctuations as the mixture becomes more acetone rich.

From this binary mixture data, the ternary system behavior could be predicted. The van Laar model is chosen to predict the ternary behavior of the mixtures, as previously discussed. The van Laar parameters calculated and tabulated in **Table 5** are used to determine the activity coefficient of each mixture component in ternary mixture, which is shown in **Eq. 13**, where 1, 2 and 3 refers to acetone, methanol and ethanol respectively.

$$\ln \gamma_1 = \frac{\left\{x_2^2 A_{12} \left(\frac{A_{21}}{A_{12}}\right)^2 + x_3^2 A_{13} \left(\frac{A_{31}}{A_{13}}\right)^2 + x_2 x_3 \frac{A_{21} A_{31}}{A_{12} A_{13}} (A_{12} + A_{13} - A_{23} \frac{A_{12}}{A_{21}})\right\}}{\left[x_1 + x_2 \left(\frac{A_{21}}{A_{12}}\right) + x_3 \left(\frac{A_{31}}{A_{13}}\right)\right]^2} \quad \text{Eq. 13}$$

From **Eq. 13**, γ_2 could be solved by interchanging 1 and 2, while solving for γ_3 by interchanging 1 and 3. From here, the relationship between the temperature and K factor over the specified mole fraction could be determined the same way in MATLAB as previously done on binary mixtures. This examination is done in **Figure 10** below, which shows the contour plot of the ternary system for K factor of 1.

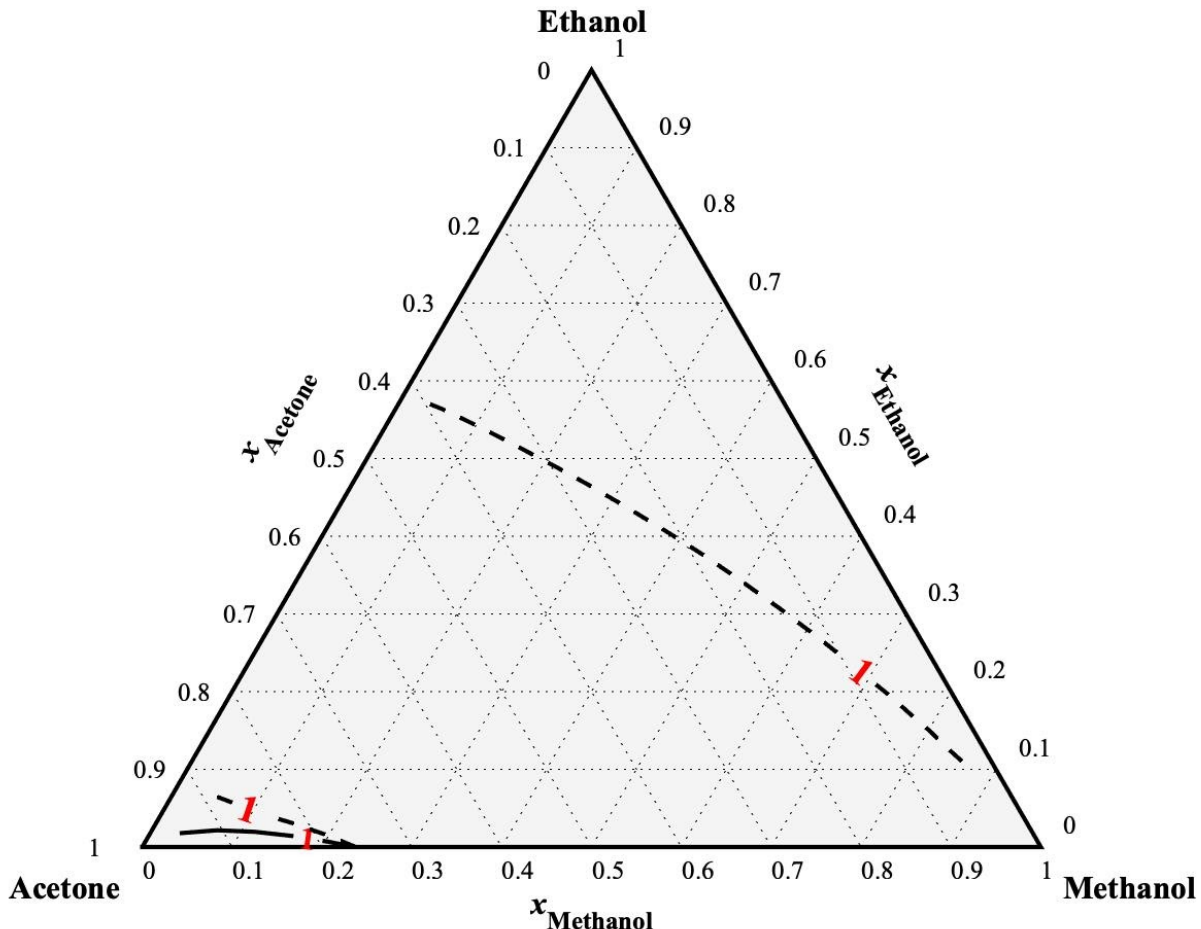


Figure 10: Ternary diagram of contour plots of $K = 1$ (— $K_{\text{Ace}} = 1$, --- $K_{\text{Met}} = 1$) of the ternary mixture at $P = 1.0271$ bar.

Figure 10 shows $K = 1$ contours for the acetone and methanol components in the ternary mixture while the ethanol component does not have a $K = 1$ contour. Based on the diagram, it is apparent that the AM mixture forms an azeotrope at $x_{\text{Met}} = 0.24$ ($x_{\text{Ace}} = 0.76$) due to the contour lines for those components intersecting at that point on the axis where $x_{\text{Eth}} = 0$. This is then confirmed by the above **Figure 7** which shows an azeotrope for the AM mixture in the same range. However, the AE and ME mixture do not form an azeotrope as there is no intersection of any contour lines where the ethanol mole fraction is above zero. This is also seen in the above

Figure 8 and **Figure 9**, where ME and AE do not form an azeotrope in the binary mixture. Since all three contour lines do not intersect with each other at a single point, there is no azeotrope formed for the ternary mixture. Further analysis of the ternary mixture is done in **Appendix K**, where contour plots for various K factors for each component can be found. The data show which molar compositions for each component have K factors approaching 1 causing potential difficulty in distillation. These plots elucidate how acetone has K factors approaching 1 on the bottom left of **Figure K1**, methanol has K factors approaching 1 in the middle and on the bottom left of **Figure K2**, and ethanol does not have any K factors approaching 1 based on **Figure K3**. This data allows for the distillation to avoid compositions with difficult to separate mixtures leading to better distillation overall. Due to this, the distillation process will be slightly easier as separating out ethanol when compared to the other two components will not have any overlap between components or phases. For further analysis of the ternary mixture to examine behavior at different temperature profiles, **Figure 11** shows the contour plot of various temperatures and the corresponding mole fractions in the ternary system.

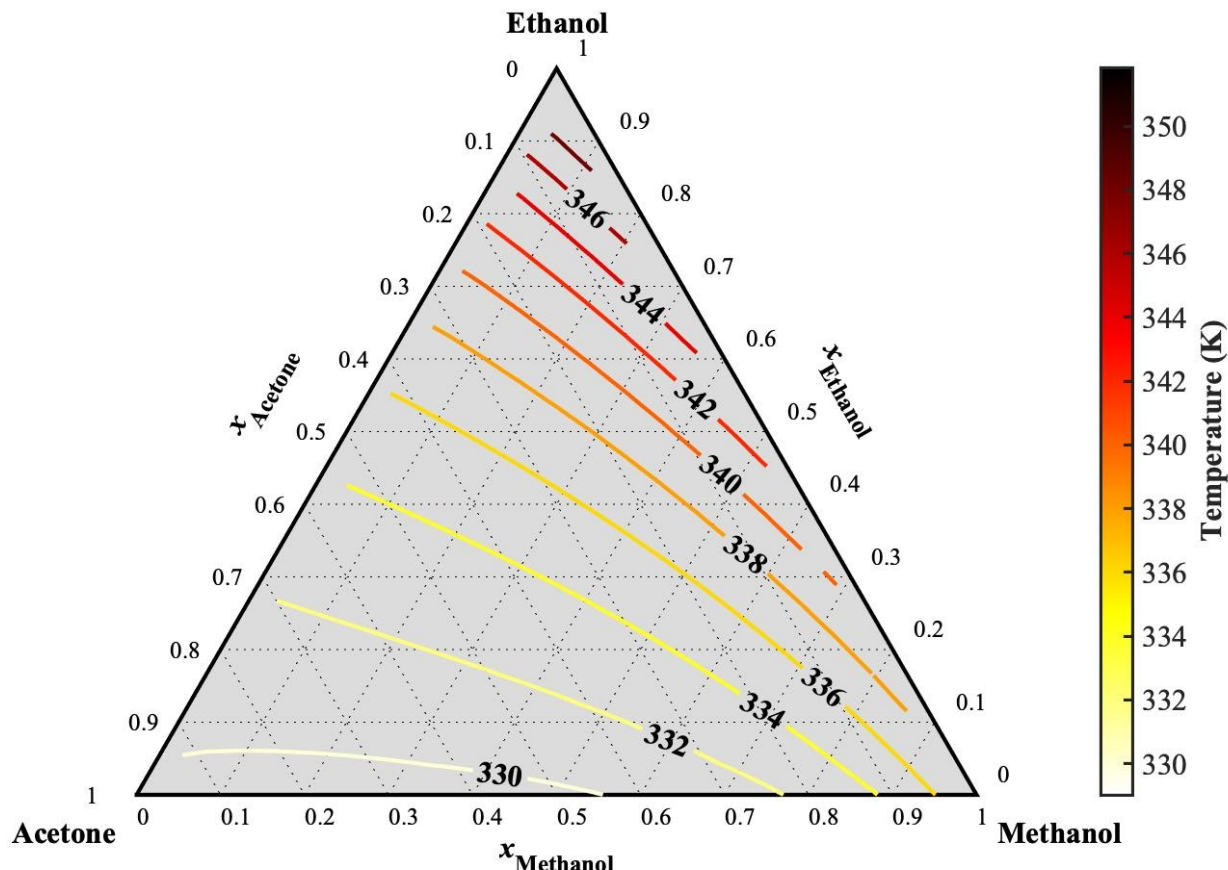


Figure 11: Ternary diagram of contour plots of various temperatures of the ternary mixture at $P = 1.0271$ bar.

Figure 11 has plotted contour lines for isotherms from the temperature range 330K - 350K as a function of liquid-phase mole fraction for each of the three components. The shape of the isotherms fits with the **Figure 10** data, as the figure shows that the ternary mixture would not have an azeotrope at any of the isotherms as they do not converge into a bulls-eye like pattern. This figure also reflects the component data boiling point at $P = 1.0271$ bar as pure components. Ethanol has the highest boiling point (351.80K), followed by methanol (338.04K), and acetone with the lowest boiling point (329.81K) at $P = 1.0271$ bar. The isotherms data follows suit with the above boiling point trend as the primarily ethanol mixtures have the highest isotherm contour lines connected to them, for example $x_{Ethanol} = 0.9$ having the isotherm at 346K, and the primarily acetone mixtures have the lowest isotherm contour lines, i.e. $x_{Acetone} = 0.97$ having an isotherm at 330K. This relationship is good for distillation as it shows that the ternary mixture can be separated into its three components based on temperature extremely well leading to successful distillation since the temperatures are determined above. A ternary diagram of temperature isosurface is included in **Appendix L** for better representation of temperature gradient in the system relative to the mole fraction of each component. The entire analysis and plots are generated from MATLAB. The codes are uploaded to Google Drive and the links are attached in **Appendix M**.

CONCLUSIONS AND RECOMMENDATIONS

In this work, isobaric VLE at $P = 1.0271$ bar for the binary systems of AM, AE, and ME and for the ternary system of acetone-methanol-ethanol are measured using a Swietoslawski ebulliometer, with the van Laar and Wilson models used for correlating the data. When analyzing the binary systems, the AM mixture forms a homogenous minimum-boiling point azeotrope at $x_{ace} = 0.763$, which is not separable by conventional distillation. A common method in practice for this separation is the extractive distillation in presence of a selective solvent, like water. However, Graczová et al. use an ionic liquid (1-Ethyl-3-methylimidazolium Trifluoromethanesulfonate) to obtain acetone with purity of 99.5 mol% and methanol with purity of above 99.0 mol%.⁶ At the same time, while the AE binary mixture does not form an azeotrope, it does have molar concentrations where the K factor approaches 1 around $x_{ace} = 0.9$ as the vapor and liquid phases begin to converge leading to difficult distillation. On top of that, the ME binary mixture does not display any molar concentrations that would cause difficulties with distillation. This lack of convergence between vapor and liquid phases in the mixture comes from the similarities of the two solvents' physical properties, where ethanol and methanol are extremely similar leading to distinct liquid and vapor curves.

With regards to pressure and temperature variations, an intensive sensitivity analysis has been conducted by factoring in variables like the building's ventilation system, depth below sea level, and plausible barometer calibration error. In industry scale distillation columns, there is limited uncontrolled variation in temperature and pressure as both parameters can affect the efficiency of the column overall. As discussed by Riggs, the temperature at the bottom of the column is set by adding heat via a reboiler, where the reboiler is controlled by the flow rates of the utility heating fluid.⁷ The temperature at the top of the distillation column is more difficult to control as the product stream is optimally in the liquid phase for storage, and as such the temperature is controlled via the reflux rate where a higher reflux rate correlates to a lower temperature at the top of the column. The pressure is maintained constant by the use of pressure controllers that directly change the amount of material in the vapor phase of the overhead or by changing the rate of condensation of the overhead. With pressure held constant, engineers change the temperature in the column to change the composition of the product stream. This emulates our experiment quite well due to it being done at isobaric conditions with the variations of temperature and a slight change in pressure taken into account to lead to the most accurate assessment. Based on this accurate assessment above, the van Laar model offered the best fit for the experimental data and as such used to plot the ternary phase diagram with contour lines for $K = 1$ and various isotherms. These figures elucidated the behavior of the ternary system under isobaric conditions and showed that an azeotrope does not exist for the ternary system and only one binary azeotrope of acetone-methanol exists. This means that the distillation for the ternary mixture is possible and will be able to separate all three components with great success according to their differences in relative volatility.

Moving forward, some improvements can be made to this lab to minimize the effect of the temperature and pressure offsets as well as ways to minimize the uncertainty in the reported data. If all experimental data was collected on the same day, the pressure and temperature offsets would be the same and the uncertainty between any calculations between the different experiments would be minimized due to there being less error propagated through fewer equations. To avoid uncertainty overall, the experimental results with higher percentages of mass loss such as methanol injected into acetone and ethanol injected into acetone should be rerun to obtain more accurate mass data leading to overall higher accuracy in the data. Another potential improvement for this lab is in the decision for which model to continue to use for the ternary system. In this report, it was done based on visual data analysis when compared to literature and experimental data. However, a more accurate method may have been to use different statistical tools to determine if the data trends are as accurate mathematically as they look visually and to determine if a model can predict specific values within a certain realm of confidence.

REFERENCES

- ¹ Wrenn, S.P; Lusvardi, V.S.; Whitmyre, G.; Buttrey, D.J. Vapor-Liquid Equilibria in the Undergraduate Laboratory. *Chemical Engineering Education*. **2000**, 34(1), 74-85. (accessed March 3rd, 2021)
- ² Tu, C.-H., Wu, Y.-S., & Liu, T.-L. Vapor-liquid equilibria of the binary systems formed by methanol, acetone and methyl vinyl ketone at 100.0 ± 0.2 kPa. *Fluid Phase Equilibria* **1997**, 129(1-2), 129–137. doi:10.1016/s0378-3812(96)03183-4 (accessed March 15th, 2021)
- ³ Amer, H. H., Paxton, R. R., & Winkle, M. V. Methanol-Ethanol-Acetone. *Industrial & Engineering Chemistry* **1956**, 48(1), 142-146. doi: 10.1021/ie50553a41 (accessed March 15th, 2021)
- ⁴ Ilia, A. Vapor-Liquid Equilibrium Measurements in Binary Polar Systems. Diploma Thesis, Vienna University of Technology, Vienna, 2016. (accessed March 16th, 2021)
- ⁵ Ku, H.-C., & Tu, C.-H. (2005). Isobaric vapor–liquid equilibria for mixtures of acetone, ethanol, and 2,2,4-trimethylpentane at 101.3kPa. *Fluid phase Equilibria* **2005**, 231(1), 99-108. doi: 10.1016/j.fluid.2005.01.007 (accessed March 15th, 2021)
- ⁶ Graczova E., Vavrusova M. Extractive Distillation of Acetone-Methanol Mixture using 1-Ethyl-3-methylimidazolium Trifluoromethanesulfonate. *Chemical Engineering Transactions* **2018**, 70, 1189-1194. doi: 10.3303/CET1870199 (accessed March 17th, 2021)
- ⁷ Riggs, J. Distillation Column Control.
<https://controlguru.com/distillation-major-disturbances-first-level-control/> (accessed March 17th, 2021)
- ⁸ NIST Office of Data and Informatics. NIST Chemistry WebBook, SRD 69. <https://webbook.nist.gov/> (accessed Feb 25th, 2021).

APPENDICES

Appendix A - Activity Coefficient Predicted by UNIFAC and van Laar Model for Each Binary

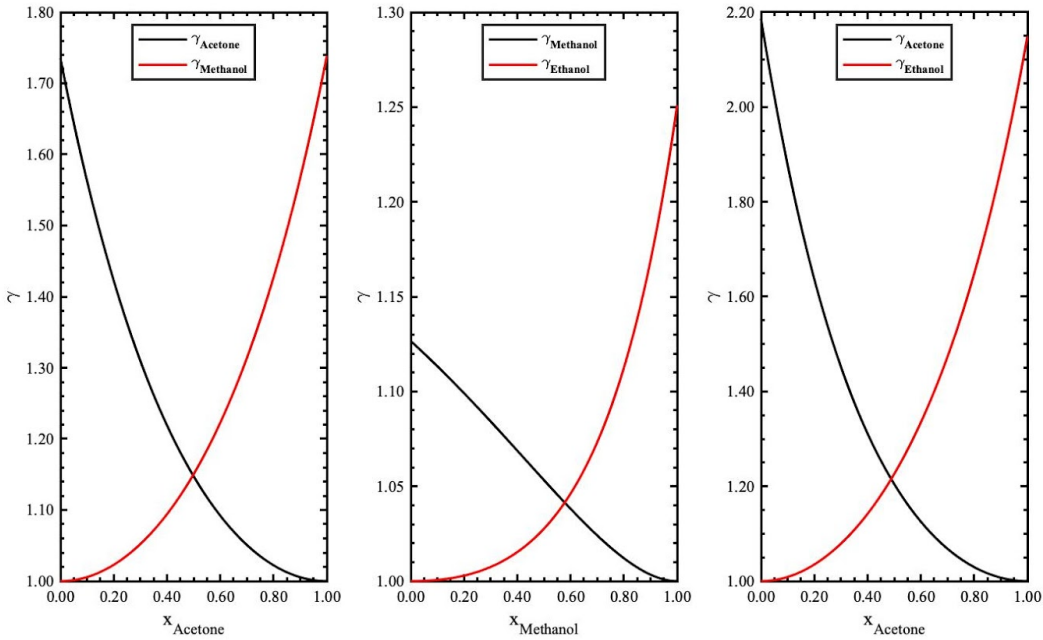


Figure A1: Activity Coefficient of Each Binary Pair by UNIFAC Method. AM, ME, and AE respectively.

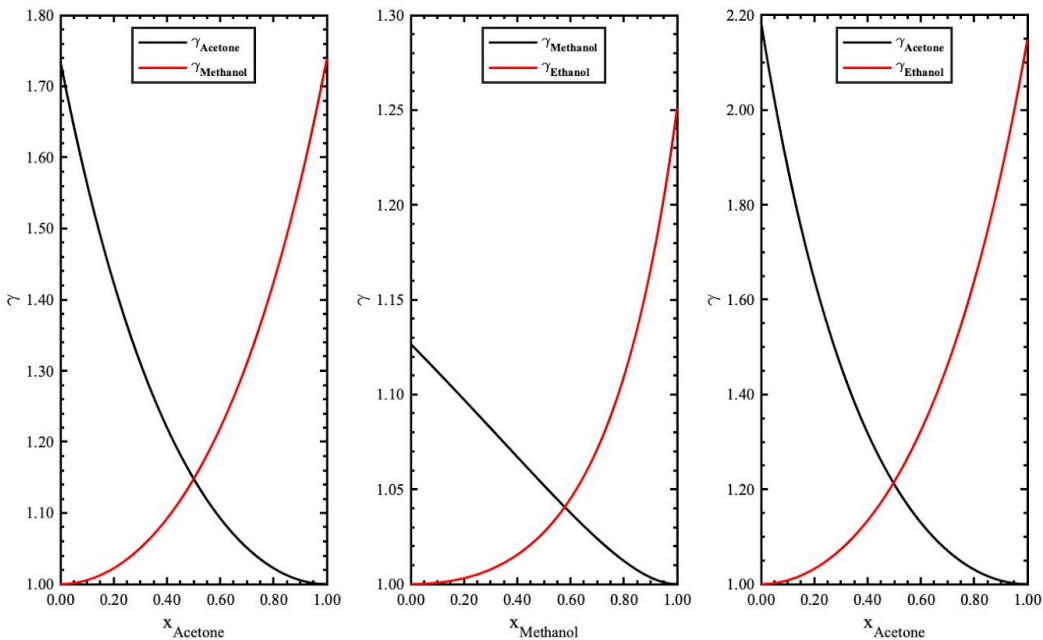


Figure A2: Activity Coefficient of Each Binary Pair by van Laar Method. AM, ME, and AE respectively.

Appendix B - Quadratic Fitting of van Laar Model with Sinusoidal Error in Fitting

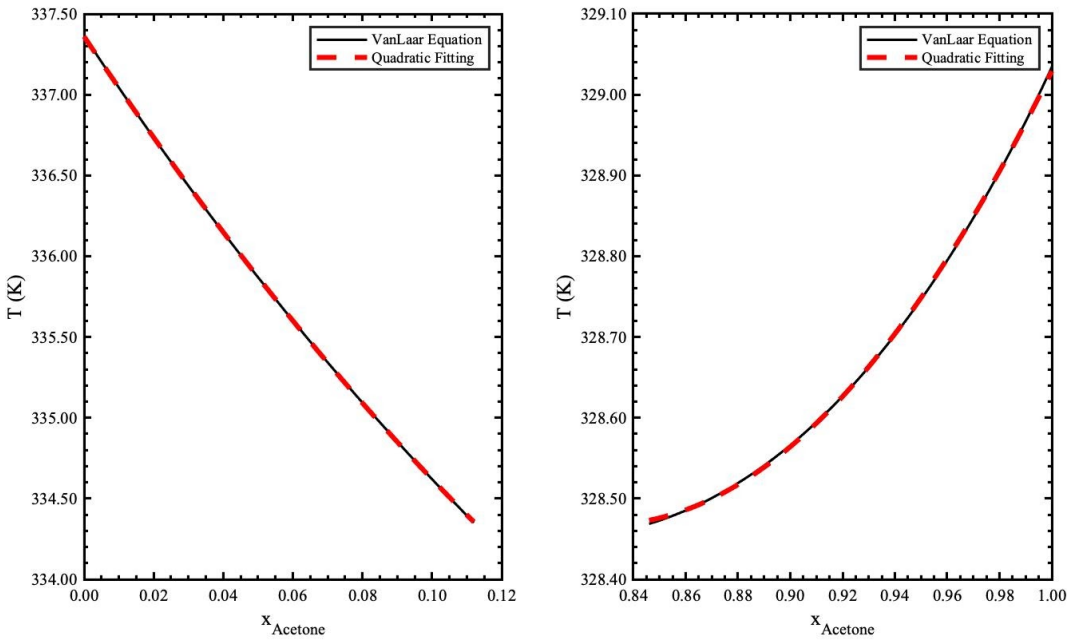


Figure B1: Fitted Quadratic Model to van Laar Equation of AM mixture pre-lab.

$$0 \leq x_{\text{Ace}} \leq 0.112 : T = 47.84x_{\text{Ace}}^2 - 32.20x_{\text{Ace}} + 337.36$$

$$0.846 \leq x_{\text{Ace}} \leq 1 : T = 19.23x_{\text{Ace}}^2 - 31.89x_{\text{Ace}} + 341.69$$

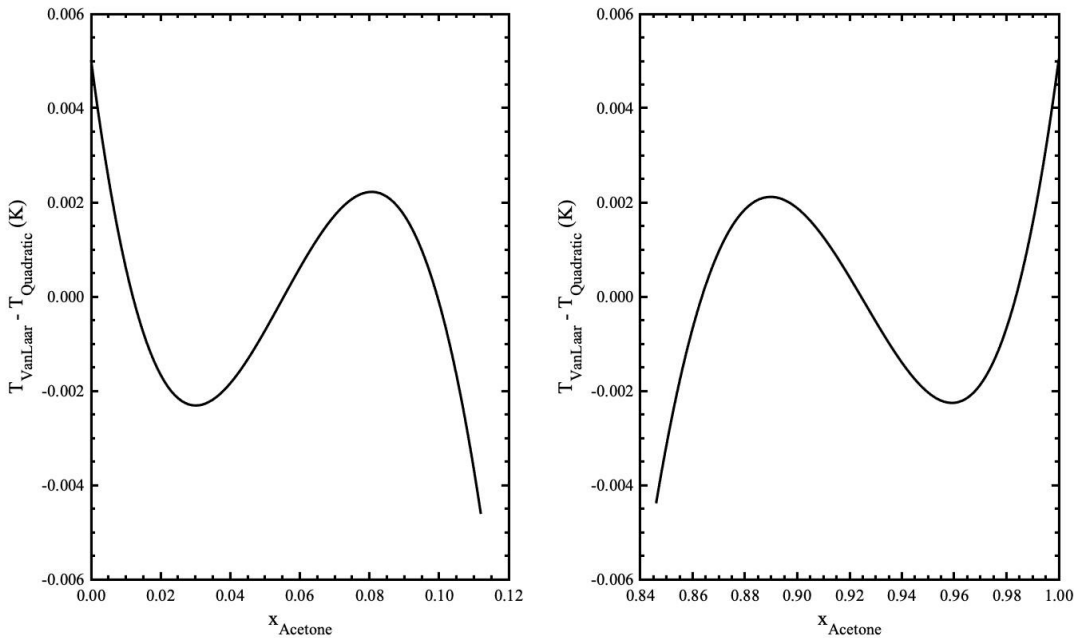


Figure B2: Sinusoidal Plot of Error in Fitting for AM mixture pre-lab.

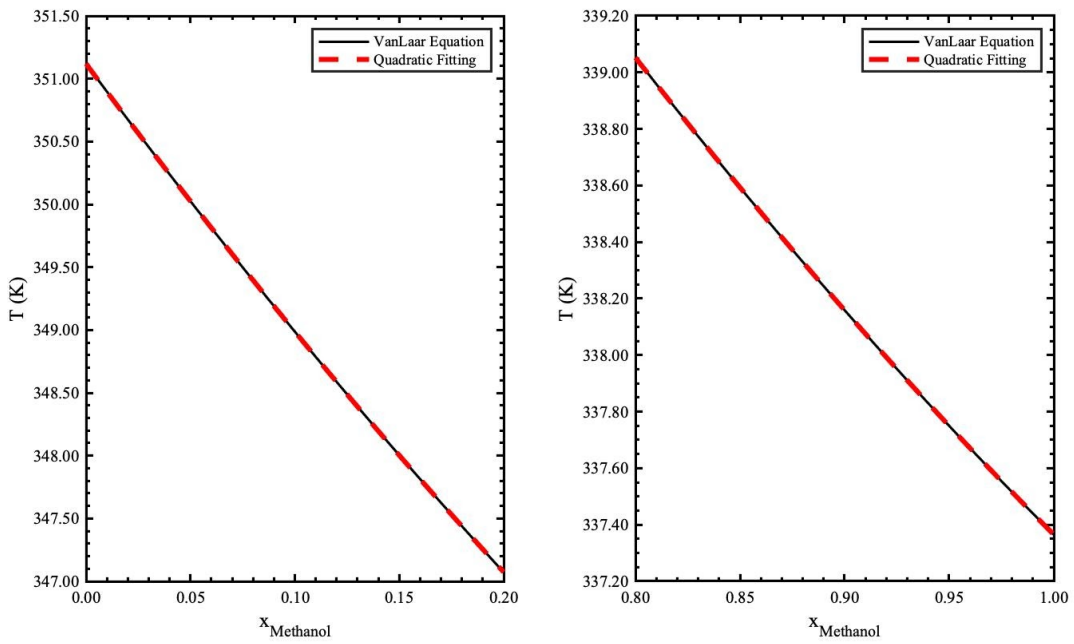


Figure B3: Fitted Second Order Polynomial to van Laar Equation of ME mixture pre-lab.

$$0 \leq x_{Met} \leq 0.2 : T = 10.93x_{Met}^2 - 22.41x_{Met} + 351.12$$

$$0.8 \leq x_{Met} \leq 1 : T = 4.98x_{Met}^2 - 17.40x_{Met} + 349.79$$

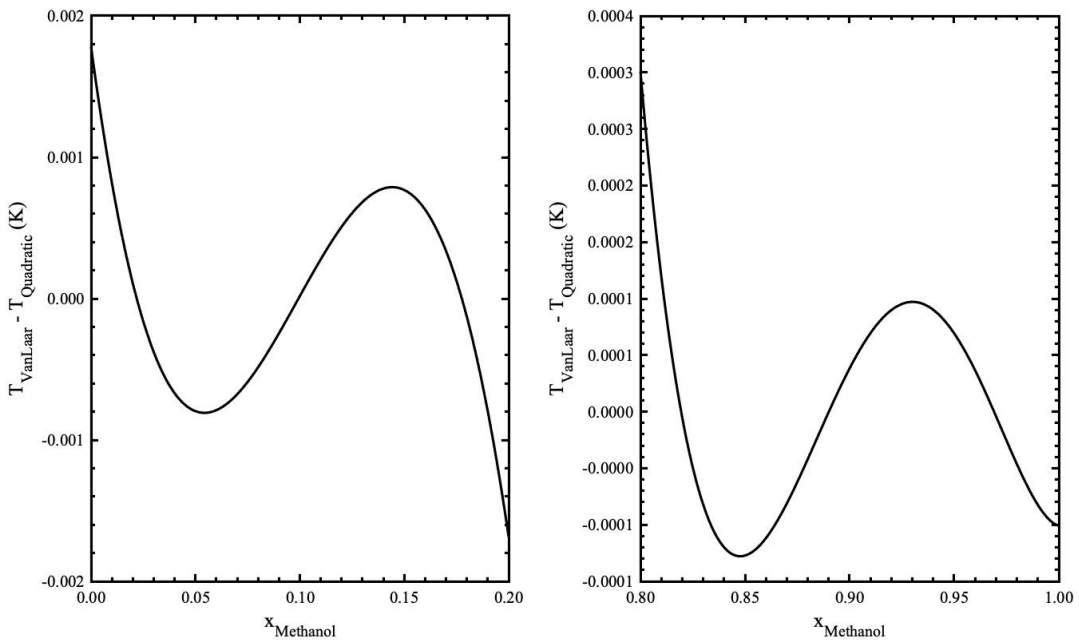


Figure B4: Sinusoidal Plot of Error in Fitting for ME mixture pre-lab.

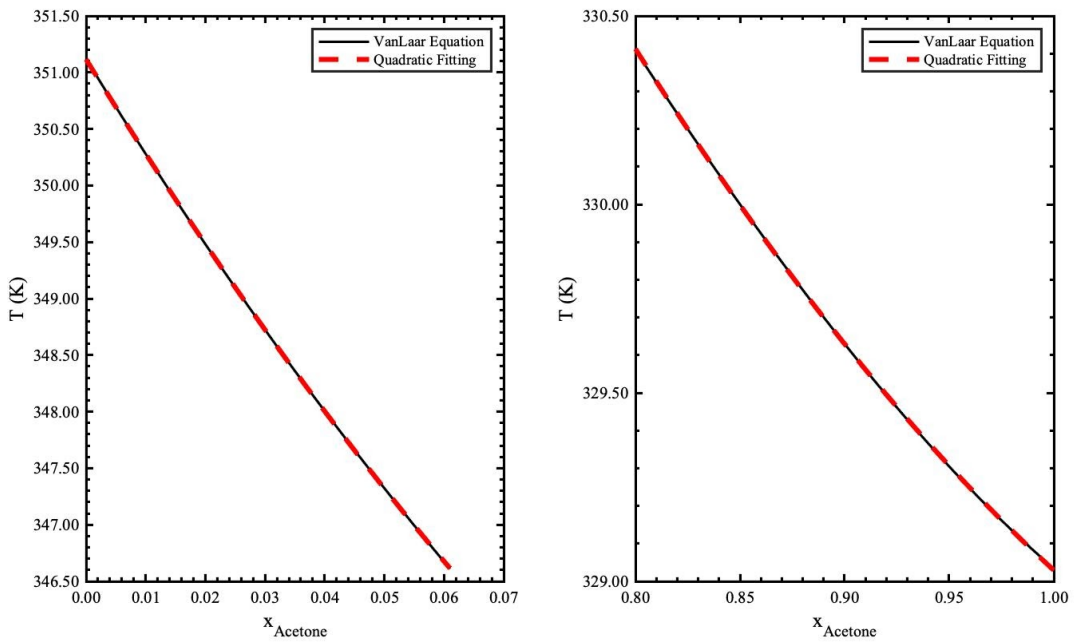


Figure B5: Fitted Second Order Polynomial to van Laar Equation of AE Mixture pre-lab.

$$0 \leq x_{\text{Ace}} \leq 0.061: T = 191.32x_{\text{Ace}}^2 - 85.45x_{\text{Ace}} + 351.12$$

$$0.8 \leq x_{\text{Ace}} \leq 1 : T = 9.13x_{\text{Ace}}^2 - 23.35x_{\text{Ace}} + 343.25$$

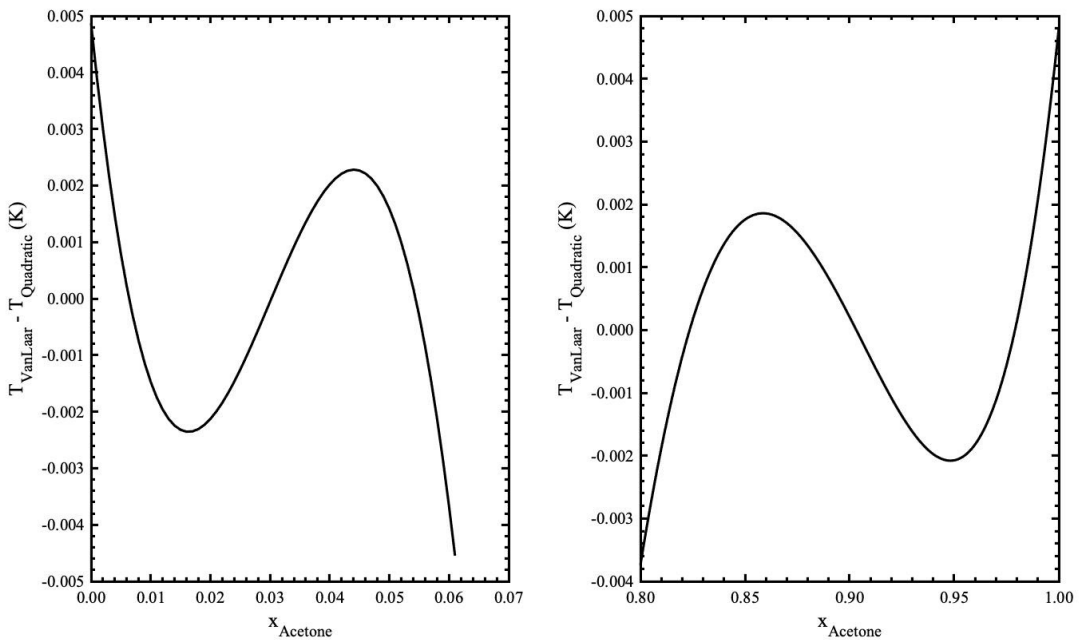


Figure B6: Sinusoidal Plot of Error in Fitting for A mixture pre-lab.

Appendix C: Poynting Pressure and Fugacity Coefficient Corrections

Before analyzing each binary mixture individually, the Poynting pressure and fugacity coefficient correction were computed to determine whether they are insignificant enough to be ignored or too significant that it should be included in the analysis calculations. **Figure C1** shows the Poynting pressure correction of each compound within a temperature range of 320K - 360K.

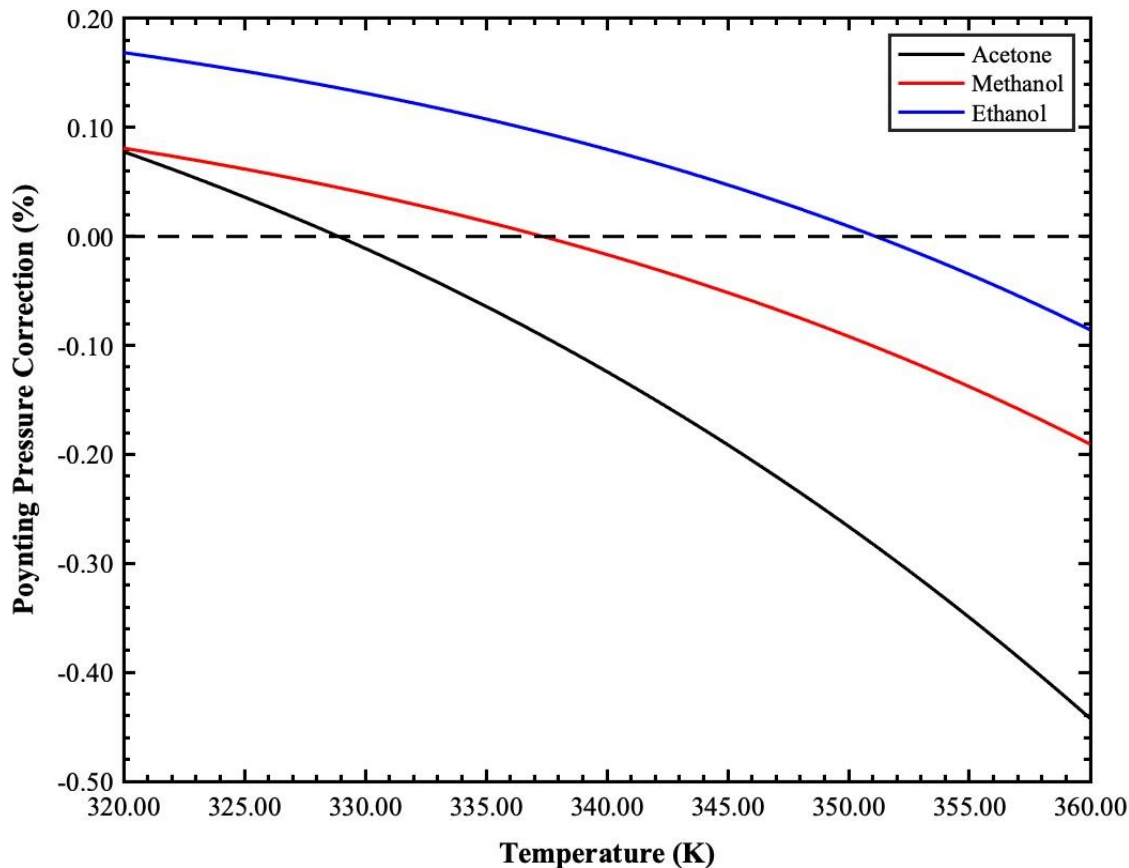


Figure C1: Poynting Pressure Correction for All Compounds within 320K - 360K.

As illustrated in **Figure C1** above, it is shown that the maximum absolute Poynting pressure correction is about 0.5% absolute difference in the calculation. Since the percentage differences are less than 1%, the Poynting correction term in Eq. 2 could be ignored in later calculations. **Figure C2** shows the fugacity coefficient correction over a temperature range of 320K - 360K for each compound.

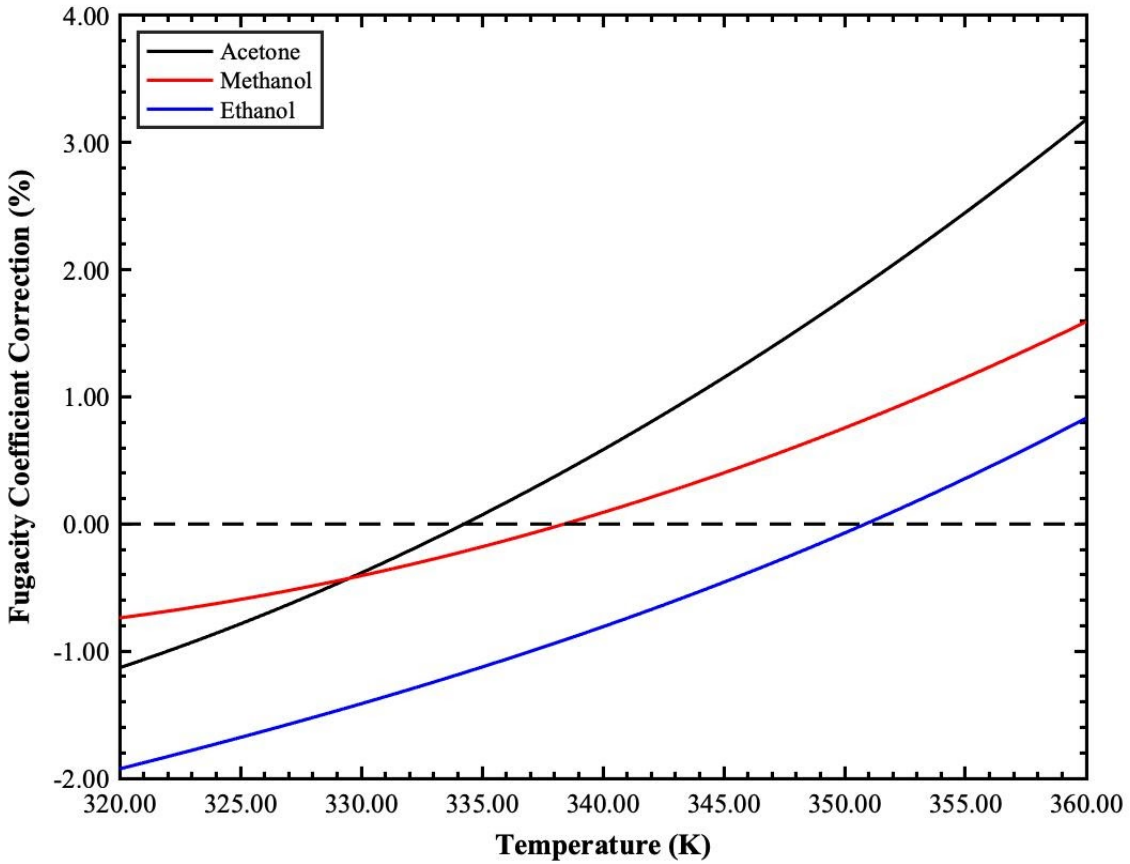


Figure C2: Fugacity Coefficient Correction at Varying Temperature for Each Compound.

The fugacity coefficient corrections were determined in ASPEN by using the Peng-Robinson equation of state. Φ_i^V were calculated based on the vapor fugacities of pure species. The pure species fugacities do not vary too much from the species fugacities in a mixture, so the pure species fugacities could be used to determine whether the corrections could be ignored or not. $\Phi_{sat,i}$ on the other hand were calculated from Eq. C, where $f^L(T,P)$ is the liquid fugacities of species i , also calculated in ASPEN.

$$\Phi_{sat,i} = \frac{f^L(T,P)}{P^{vap}(T) \cdot \exp \left\{ \frac{v_i^L [P_{total} - P^{vap}(T)]}{RT} \right\}} \quad \text{Eq. C}$$

The ratio of these fugacity coefficients are plotted as shown in Figure C2 and it could be seen that the corrections vary from 0 to about 3.5% in absolute value. More than 1% in correction is significant, that it should be taken into account for the corrections in the calculations. The specified temperature range was chosen based on the boiling point of the individual compound, where the binary/ternary mixtures' boiling point will lie somewhere in between the range, at a given mole fraction of each species.

Appendix D - Injection Data for All Binary Mixtures with their Associated Errors

Table D1: Injection Data and Error Propagation of AM mixture.

Inj. #	A/M (solute/solvent)				M/A (solute/solvent)				P (bar)	σ_P (bar)
	T (°C)	σ_T (°C)	x	σ_x	T (°C)	σ_T (°C)	x	σ_x		
1	64.68	0.32	0.01638	0.00002	56.22	0.03	0.0344	0.0001	1.0241	0.0002
2	63.78		0.03114	0.00003	56.01		0.0665	0.0001		
3	63.01		0.04637	0.00003	55.85		0.0983	0.0001		
4	62.43		0.06111	0.00004	55.79		0.1282	0.0001		
5	61.97		0.07329	0.00004	55.72		0.1552	0.0001		

Table D2: Injection Data and Error Propagation of ME mixture.

Inj. #	M/E (solute/solvent)				E/M (solute/solvent)				P (bar)	σ_P (bar)
	T (°C)	σ_T (°C)	x	σ_x	T (°C)	σ_T (°C)	x	σ_x		
1	77.97	0.06	0.02026	0.00005	64.99	0.03	0.01221	0.00003	1.0281	0.0001
2	77.48		0.03913	0.00007	65.09		0.02373	0.00003		
3	77.12		0.05678	0.00008	65.16		0.03414	0.00004		
4	76.72		0.07573	0.00010	65.22		0.04331	0.00005		
5	76.34		0.09228	0.00011	65.28		0.05174	0.00005		

Table D3: Injection Data and Error Propagation of AE mixture.

Inj. #	A/E (solute/solvent)				E/A (solute/solvent)				P (bar)	σ_P (bar)
	T (°C)	σ_T (°C)	x	σ_x	T (°C)	σ_T (°C)	x	σ_x		
1	77.57	0.16	0.01200	0.00003	56.98	0.32	0.03073	0.00004	1.0293	0.0003
2	76.39		0.02297	0.00004	57.15		0.05924	0.00006		
3	75.67		0.03204	0.00005	57.36		0.08445	0.00007		
4	74.91		0.04039	0.00006	57.53		0.10974	0.00008		
5	74.35		0.04758	0.00006	57.65		0.13330	0.00009		

The error propagations tabulated in **Table D1 - D3** were calculated based on **Eq. D1 - D3** shown below.

$$\sigma_x = \sqrt{\sigma_a^2 + \sigma_b^2 + \sigma_c^2} \quad \text{Eq. D1}$$

$$\frac{\sigma_x}{x} = \sqrt{\frac{\sigma_a^2}{a^2} + \frac{\sigma_b^2}{b^2} + \frac{\sigma_c^2}{c^2}} \quad \text{Eq. D2}$$

$$\sigma_f = \sqrt{\left(\frac{\delta f}{\delta x}\sigma_x\right)^2 + \left(\frac{\delta f}{\delta y}\sigma_y\right)^2 + \left(\frac{\delta f}{\delta z}\sigma_z\right)^2 + \dots} \quad \text{Eq. D3}$$

Eq. D1 refers to error in value x, σ_x when x was determined from either addition or subtraction. **Eq. D2** on the other hand refers to σ_x when x was computed from either multiplication or division. **Eq. D3** is the general approach to error propagation determination for value f, which is a function of x, y, z, etc. **Eq. D3** is used mainly to determine the error in temperature and pressure from Antoine equations, as well as van Laar and Wilson models' parameters.

Appendix E - Variations between Atmospheric and Lab Pressure

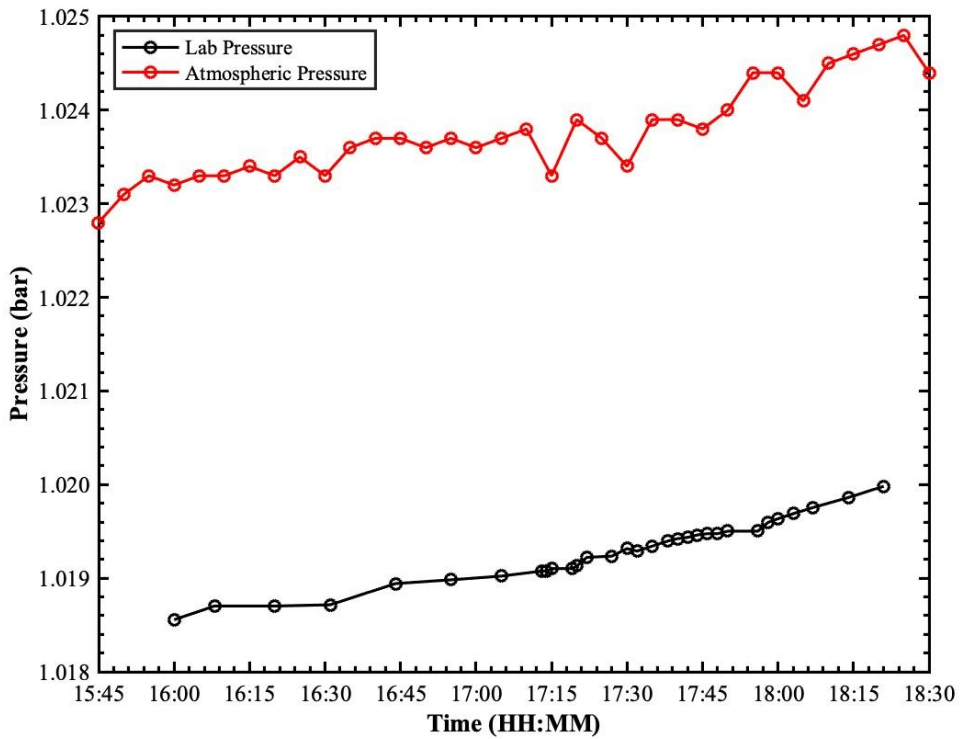


Figure E1: Recorded Lab Pressure and Atmospheric pressure vs Time on February 25th, 2021.

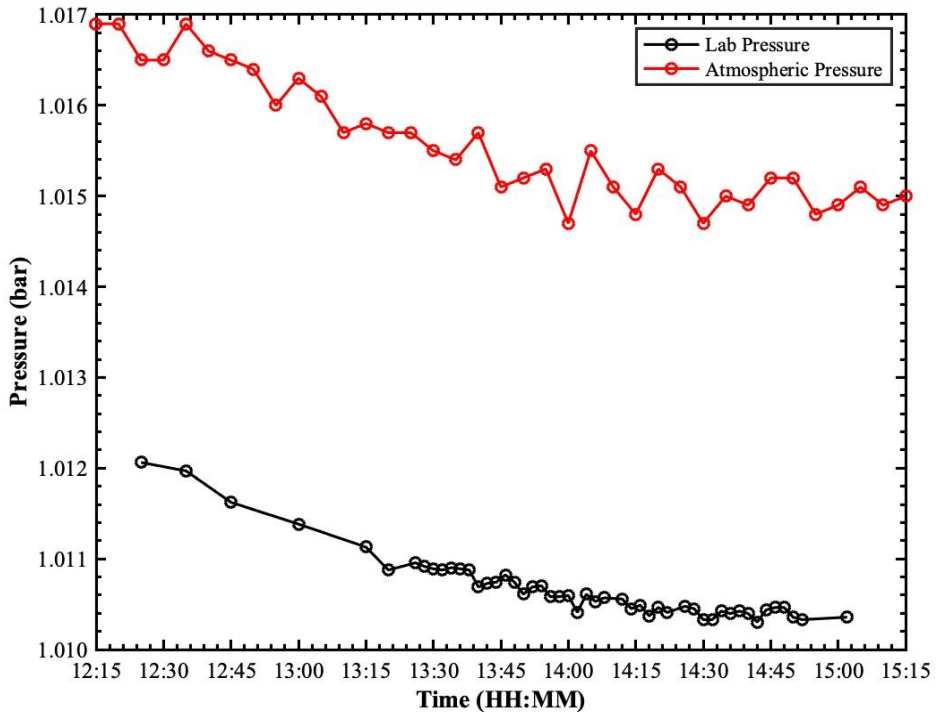


Figure E2: Recorded Lab Pressure and Atmospheric pressure vs Time on March 5th, 2021.

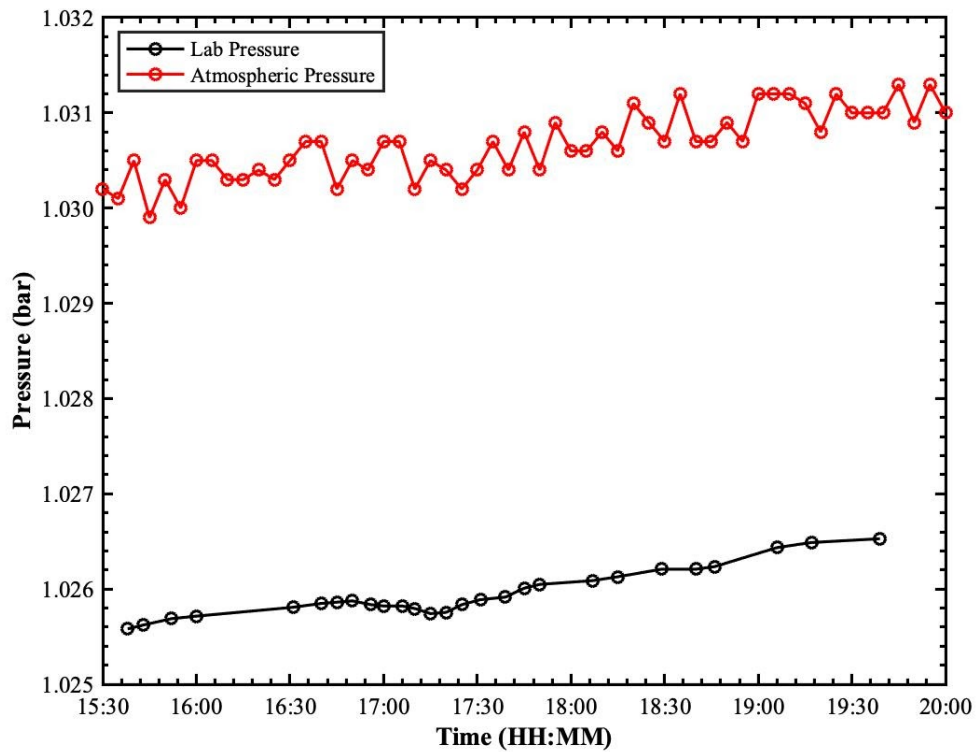


Figure E3: Recorded Lab Pressure and Atmospheric Pressure vs Time on March 8th, 2021.

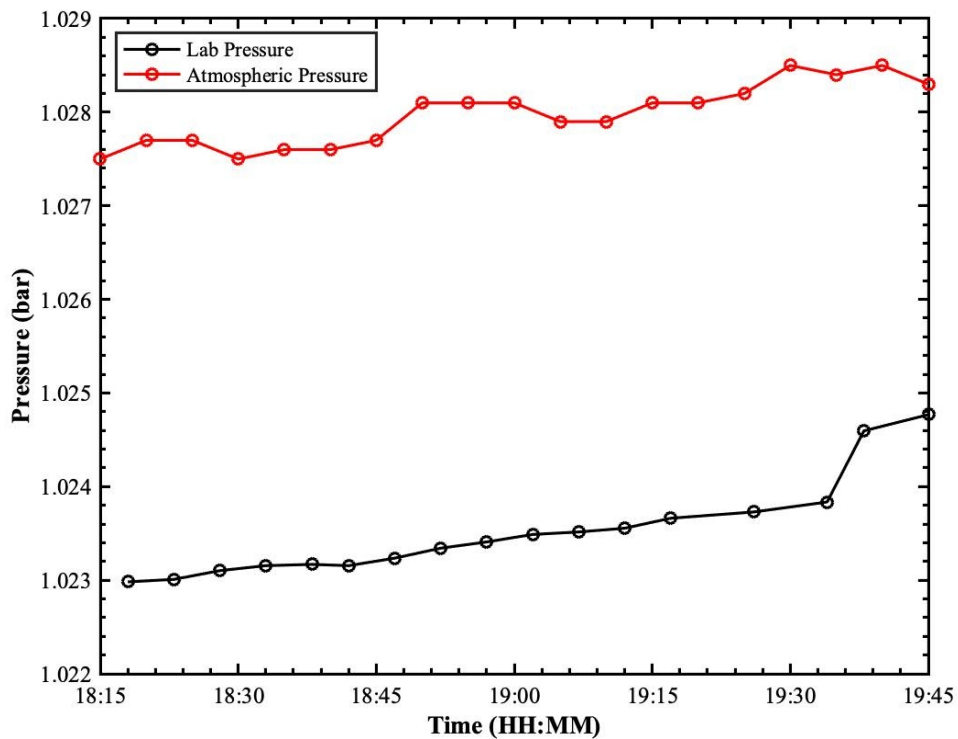


Figure E4: Recorded Lab Pressure and Atmospheric Pressure vs Time on March 9th, 2021.

It could be seen that on Feb. 25th and Mar. 8th (**Figure E1 and E3**), the laboratory pressure is nearly uniform while the experiment is being performed. However, there are a few fluctuations in the atmospheric measurements because of weather conditions. On Mar. 5th (**Figure E2**), the lab pressure gradient is decreasing over time, which can either be due to calibration error or the building's ventilation system. Whereas, the atmospheric pressure decreases because of warm weather conditions. On top of that, on Mar. 9th (**Figure E4**), the laboratory pressure follows a linear trend until 19:35, followed by a sharp pressure increase which might correspond to a calibration error in the barometer as opposed to weather conditions, which is evident by stagnant DEOS measurements.

Appendix F - Relevant Antoine Parameters and Compound Thermodynamic Properties

Table F: Antoine Equation Parameters and Other Thermodynamic Properties.⁸

Compound	Molar Mass (g/mol)	Temperature Range (K)	Antoine Equation Parameters		
			A_t	B_t	C_t
Acetone	58.08	259.16 - 507.60	4.42448	132.253	-32.445
Methanol	32.04	288.10 - 356.83	5.20409	1581.341	-33.500
Ethanol	46.07	292.77 - 366.63	5.24677	1598.673	-46.424

Appendix G - Averaged Temperature Data for Each Binary Mixture

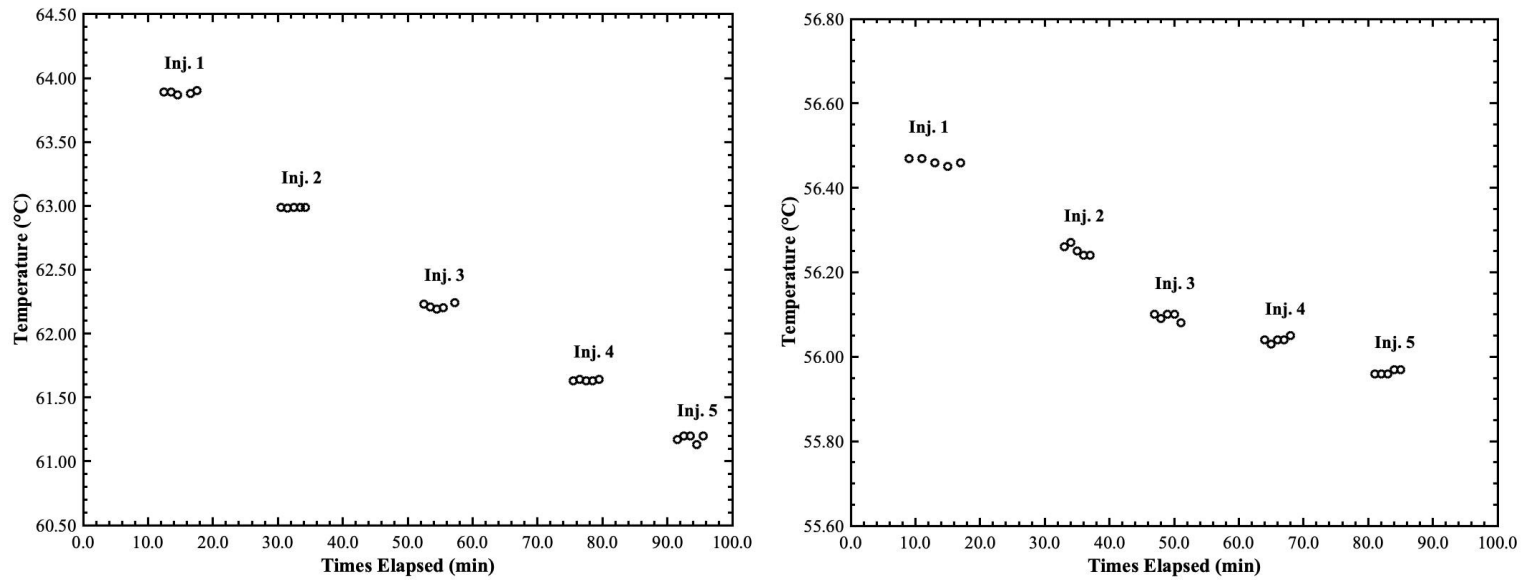


Figure G1: Various averaged temperature data at steady state as a function of time for AM mixture; a) acetone injected into methanol and b) methanol injected into acetone.

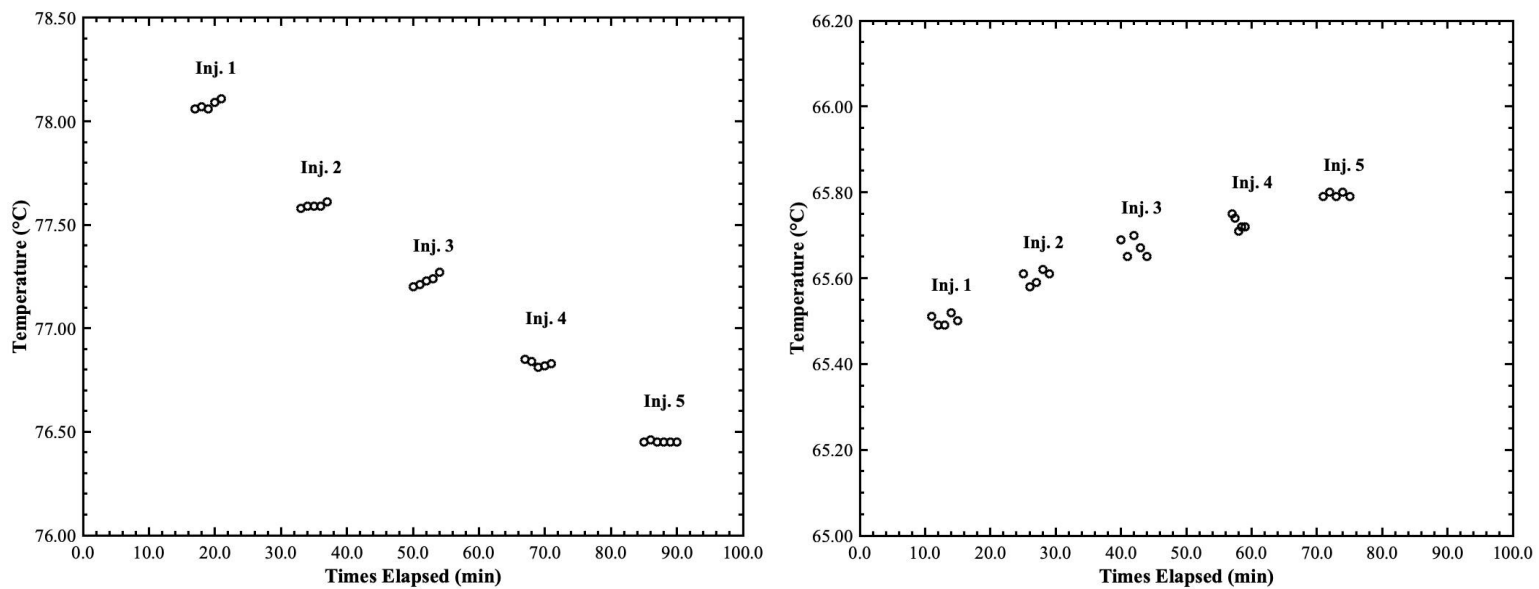


Figure G2: Various averaged temperature data at steady state as a function of time for ME mixture; a) methanol injected into ethanol and b) ethanol injected into methanol.

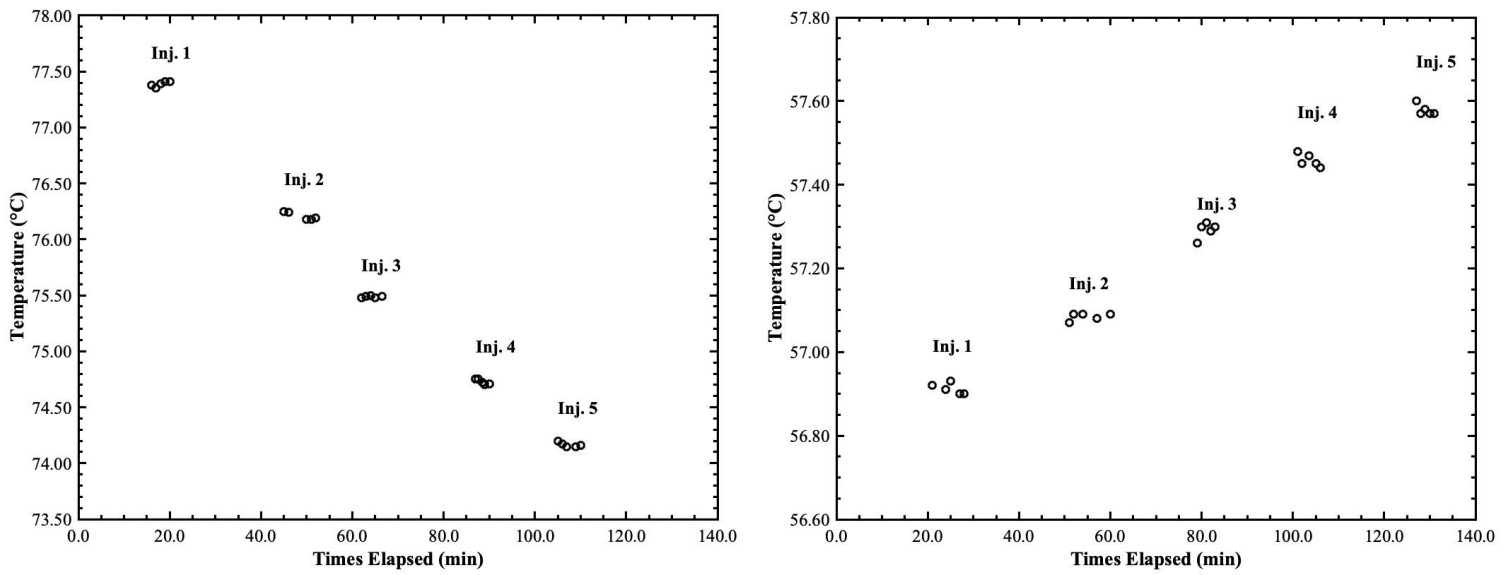


Figure G3: Various averaged temperature data at steady state as a function of time for AE mixture; a) acetone injected into ethanol and b) ethanol injected into acetone.

Figures G1 - G3 show the equilibrium temperatures of various injections of each mixture. The cluster of constant data points proves equilibrium has been achieved since the temperature is no longer changing over a range of time. The data point at the end of each injection's equilibrium will be the point where the next injection is done. For example, in **Figure G3b**, the second injection was made around the 30th minute, and it took until about the 45th minute for this injection to reach equilibrium. **Figure G2b** shows especially abnormal data. The temperatures were not extraordinarily linear perhaps because this mixture is easily separable. This means the equilibrium data is depicted around an acceptable deviation from the average for equilibrium.

Appendix H - Experimental Data Fitted to Quadratic Equation, with van Laar and Wilson Correlative Models of T-xy plots.

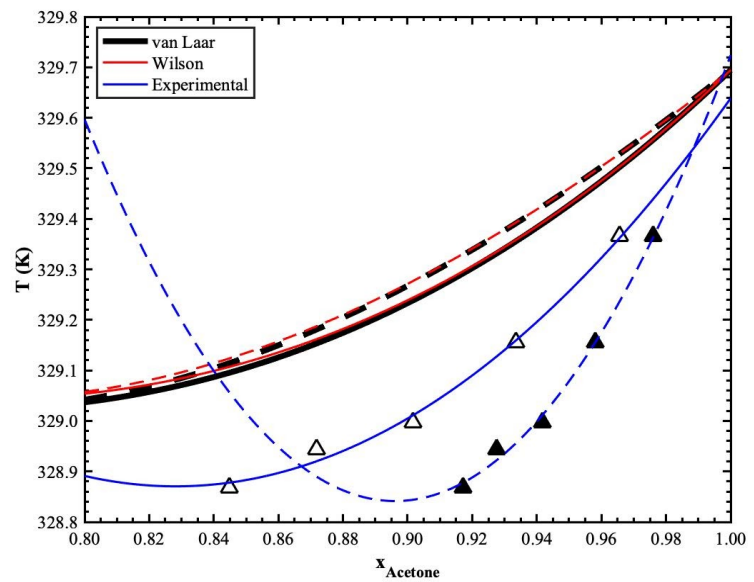
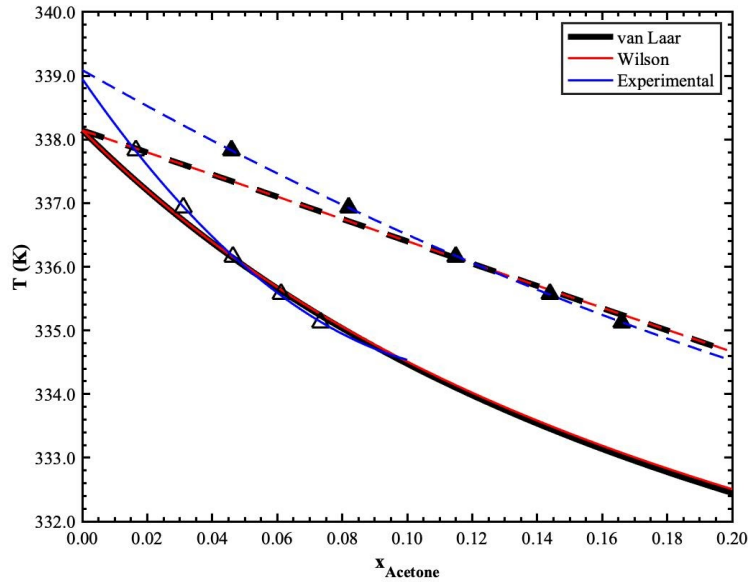


Figure H1: T-xy plot with quadratic fitting ($-x_A$, $--y_A$) of the experimental data ($\triangle - x_A$, $\blacktriangle - y_A$ at $P = 1.0271$ bar) for AM mixture; a) A injected into M (left) and b) M injected into A (right).

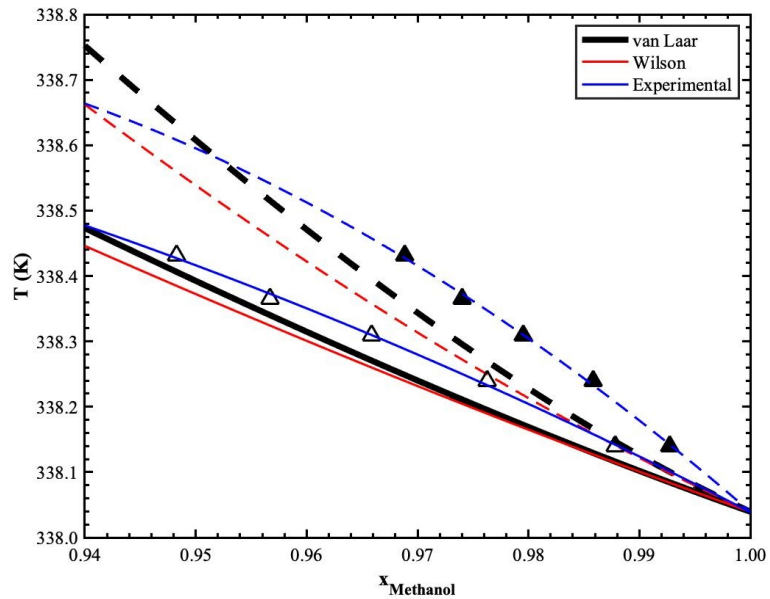
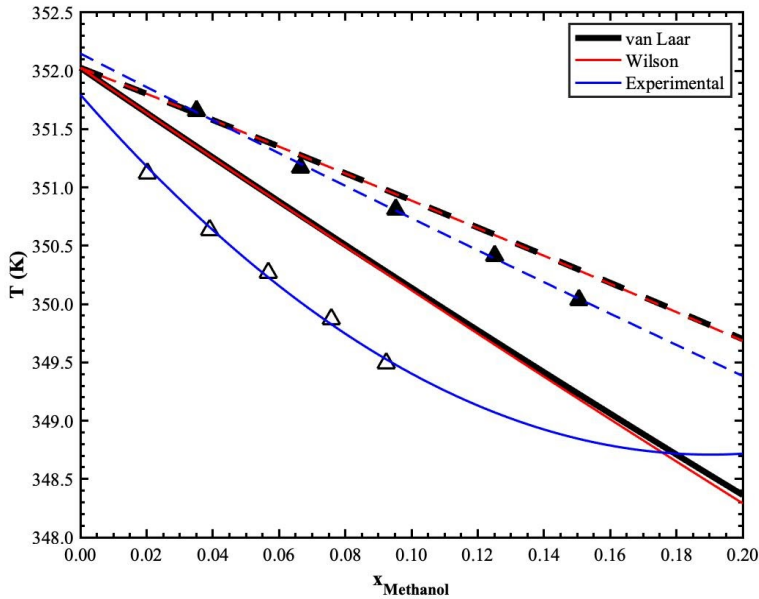


Figure H2: T-xy plot with quadratic fitting ($-x_A$, $--y_A$) of the experimental data ($\triangle - x_A$, $\blacktriangle - y_A$ at $P = 1.0271$ bar) for ME mixture; a) M injected into E (left) and b) E injected into M (right).

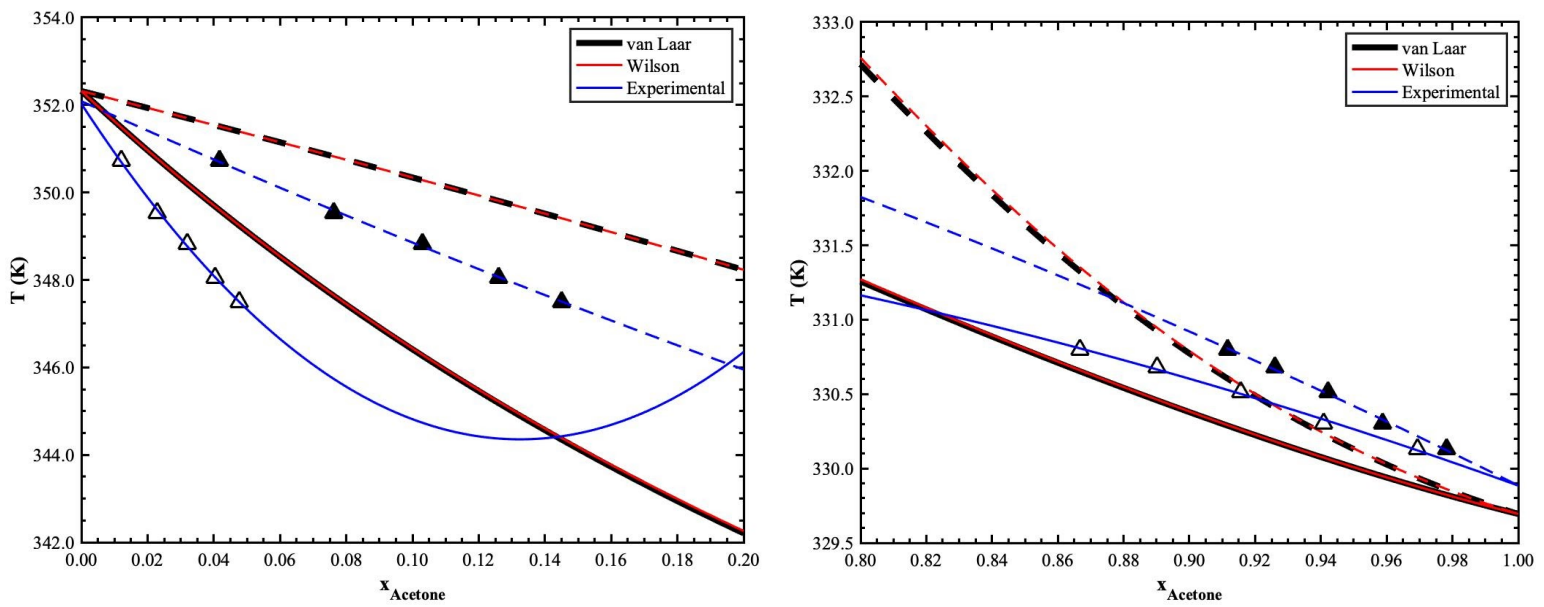


Figure H3: T-xy plot with quadratic fitting ($-x_A$, $--y_A$) of the experimental data ($\triangle - x_A$, $\blacktriangle - y_A$ at $P = 1.0271$ bar) for AE mixture; a) A injected into E (left) and b) E injected into A (right).

Figures H1 - H3 show quadratic fitting for three binary mixtures of various injections near the infinite dilution limits. In these plots, the liquid-phase experimental data have been fitted using a quadratic model pertaining to its nature in a T-xy plot near infinite dilution limits. The vapor phase experimental data were calculated based on van Laar model, and were plotted in the same figures. Looking at the fitting closely, they do not agree very much with the van Laar and Wilson model, with the exception of A injected into M as shown in **Figure H1a**. When the original data was used without any offsets applied, they are not even closely aligned with the models. Regardless of the experimental data deviations from both models, it could still accurately predict the trend demonstrated in T-xy plots, as compared to the UNIFAC predictive model attached in **Appendix I**. Quadratic fitting was used as it is a simple model that mimics the real behavior near infinite dilution limit. However, one could consider fitting the experimental data through linear relationship. As observed in **Figure H2**, the T-xy plot of van Laar and Wilson model are quite linear within the specified mole fraction range. Linear fitting the experimental data would not produce a large difference in slope when compared to quadratic fittings, in which the slope is used to determine the activity coefficients at infinite dilution. However, for consistency and lower systematic error, quadratic fitting was done for all mixtures experimental data.

Appendix I - T-xy Plots Generated Pre-lab from UNIFAC Predictive Models

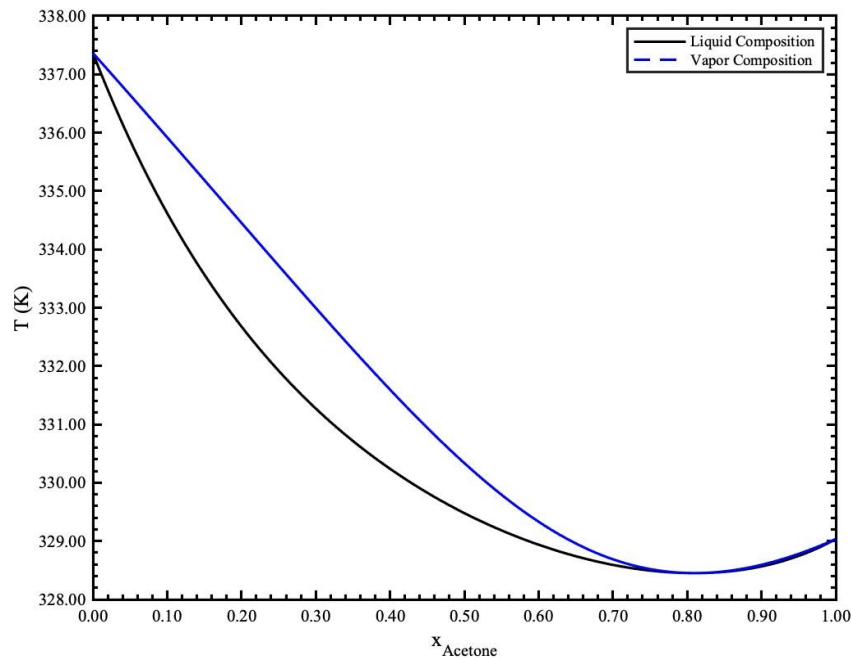


Figure I1: T-xy of AM Mixture by van Laar Method based on UNIFAC models of infinite dilution activity coefficients.

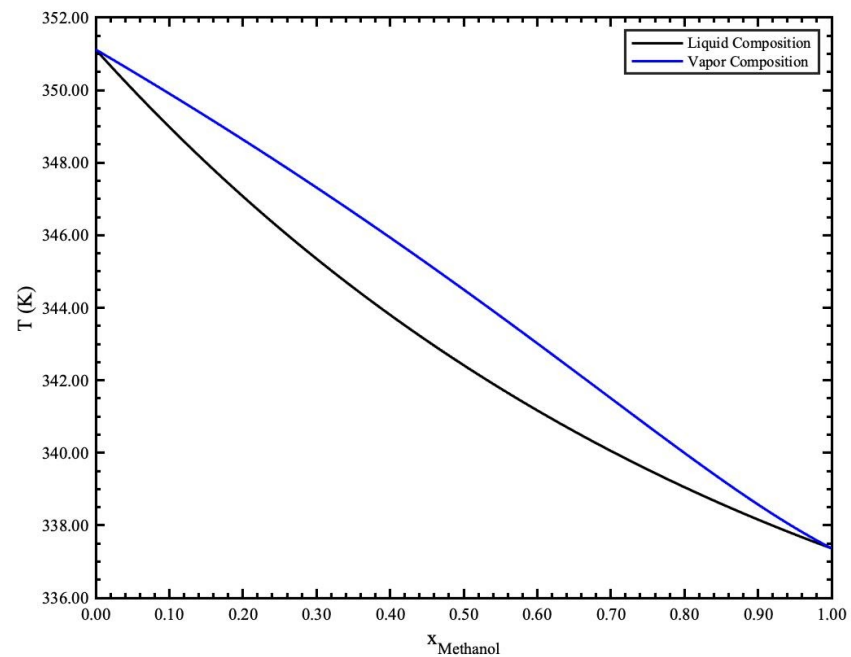


Figure I2: T-xy of ME Mixture by van Laar Method based on UNIFAC models of infinite dilution activity coefficients.

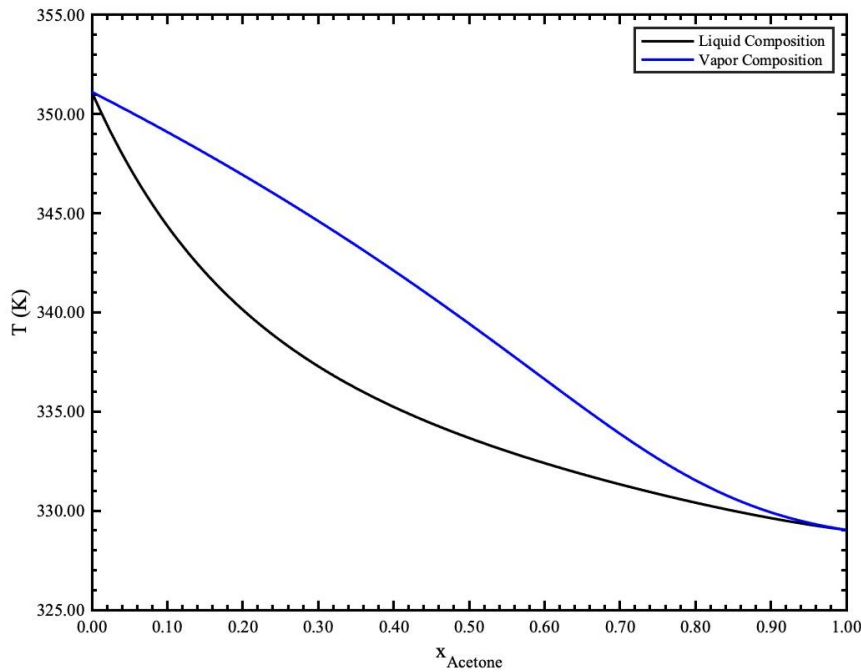


Figure I3: T-xy of AE Mixture by van Laar Method based on UNIFAC models of infinite dilution activity coefficients.

T-xy plots in **Figure I1 - I3** are generated based on the van Laar model. To determine the van Laar parameters, UNIFAC infinite dilution activity coefficients were used. There was no experimental data provided initially, so UNIFAC is a predictive model which can precisely predict the T-xy behavior of the binary mixtures. UNIFAC was used instead of other predictive models (such as Regular Solution Theory) as it took into account the variations in functional groups the compounds have. These figures are primarily used to compare the T-xy plots generated in the main report based on the experimental data, to make sure that the trend observed remains the same and does not deviate much from the UNIFAC prediction. The infinite dilution activity coefficients and van Laar parameters are as tabulated in **Appendix J** in **Table J**.

Appendix J - γ_i^∞ and van Laar Parameters from UNIFAC Predictive Models

Table J: γ_i^∞ from UNIFAC models and van Laar Parameters for pre-lab analysis.

<i>ij</i>		γ_i^∞		A_{ij}	
1	2	γ_1^∞	γ_2^∞	A_{12}	A_{21}
Acetone	Methanol	1.7351	1.7386	0.5511	0.5531
Methanol	Ethanol	1.1266	1.2509	0.1192	0.2238
Acetone	Ethanol	2.1859	2.1492	0.7820	0.7651

Appendix K - Contour Plots of the Ternary Mixture on a Ternary Plot For Each Compound

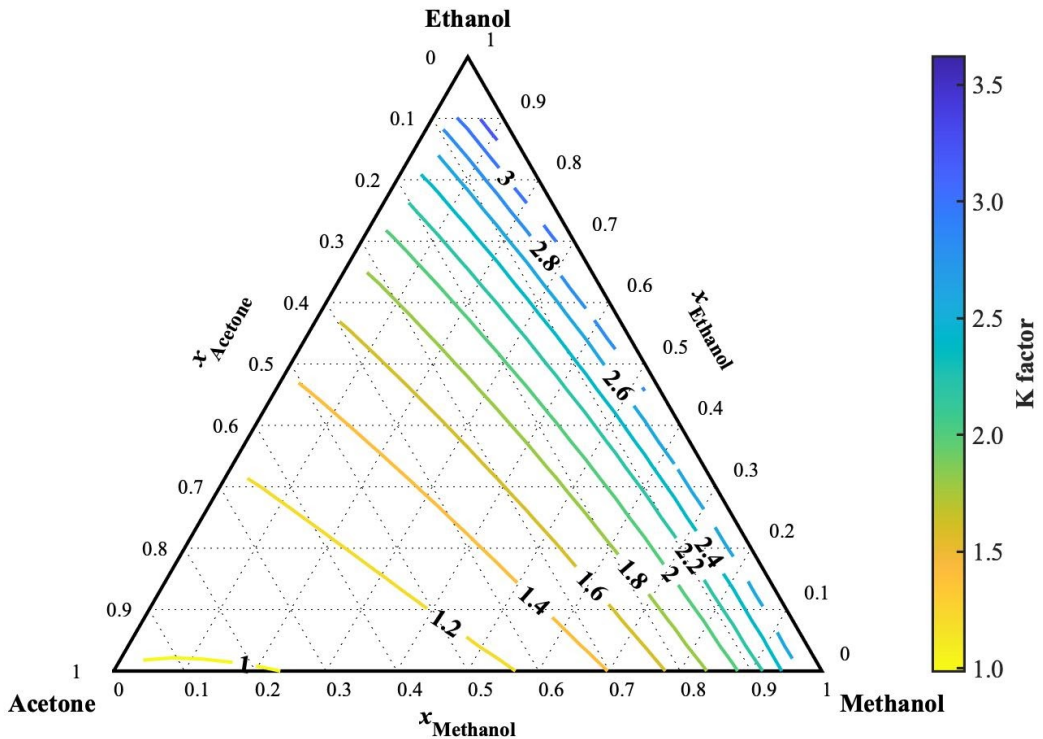


Figure K1: Ternary diagram of contour plots of various K factors of acetone of the ternary mixture at $P = 1.0271$ bar.

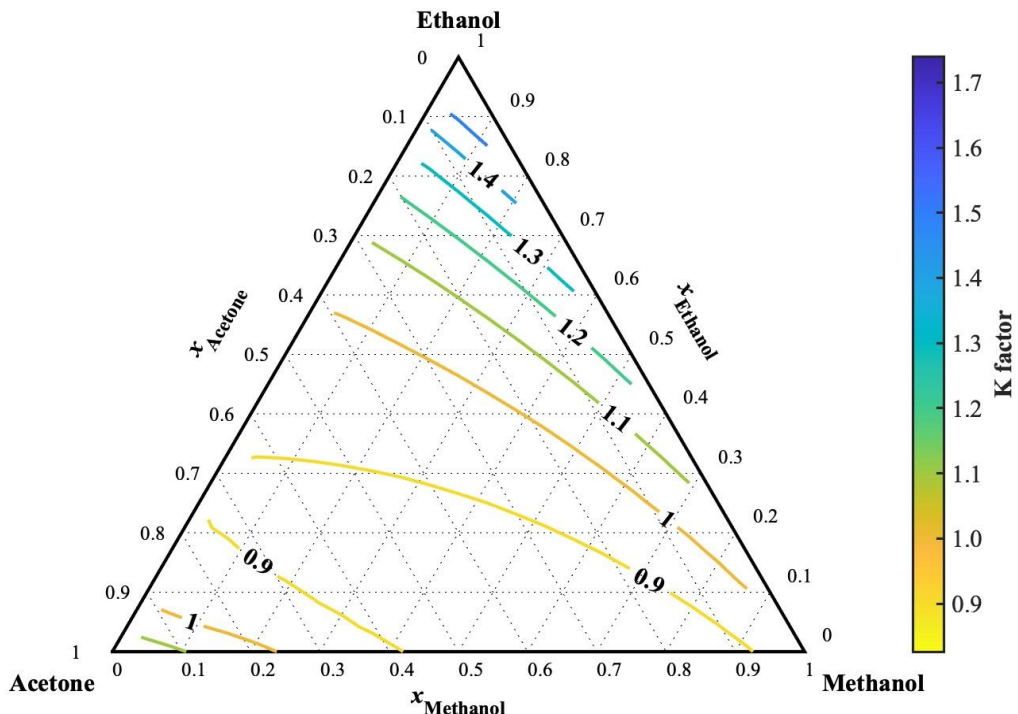


Figure K2: Ternary diagram of contour plots of various K factors of methanol of the ternary mixture at $P = 1.0271$ bar.

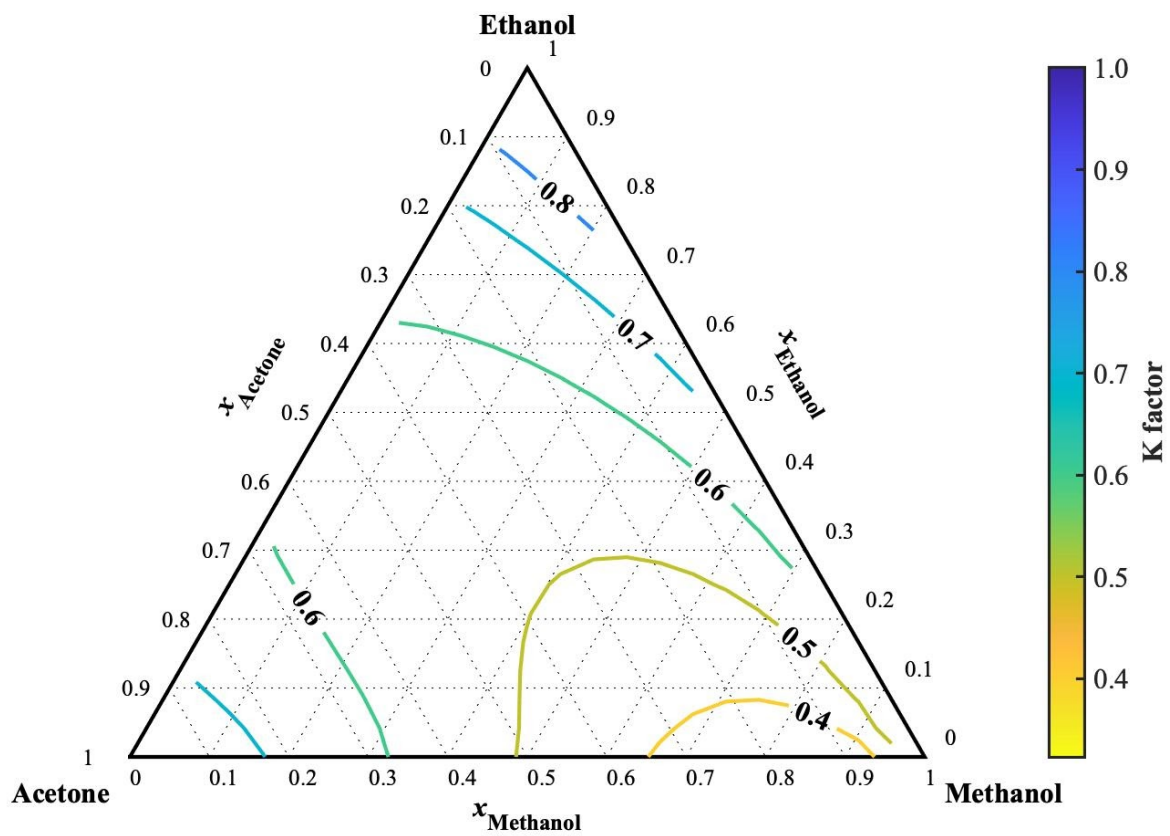


Figure K3: Ternary diagram of contour plots of various K factors of ethanol of the ternary mixture at $P = 1.0271$ bar.

Appendix L - Isosurface of the Ternary Mixture on a Ternary Plot

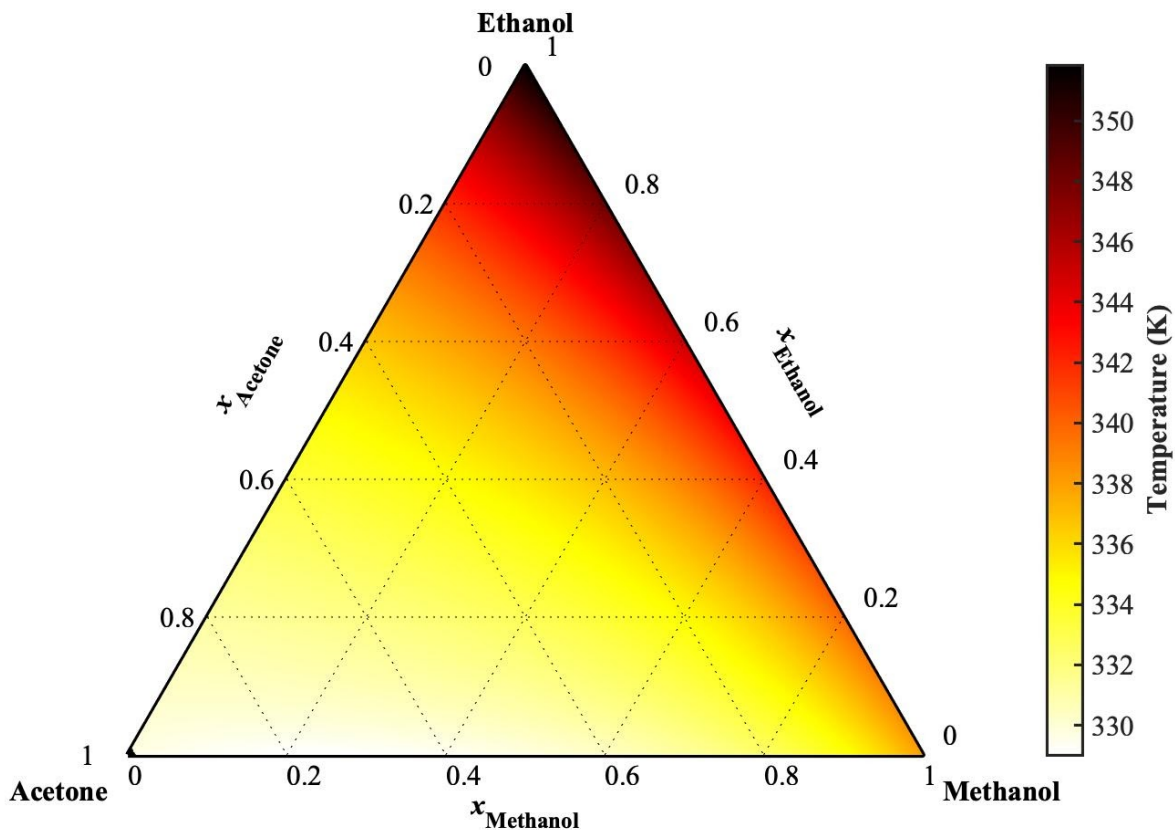


Figure L: Isosurface on a Ternary Plot of the Ternary Mixture

Appendix M - MATLAB Coding for Analysis and Plot Generations

Please follow these steps to access the MATLAB Code:

1. Access the shared google drive link [here](#).
2. Navigate to the *Matlab for Final Report* folder.